Chaotic Balanced State in a Model of Cortical Circuits

C. van Vreeswijk and H. Sompolinsky
Racah Institute of Physics and Center for Neural Computation
Hebrew University
Jerusalem, 91904 Israel

10 March 1998

Abstract

The nature and origin of the temporal irregularity in the electrical activity of cortical neurons *in vivo* are still not well understood. We consider the hypothesis that this irregularity is due to a balance of excitatory and inhibitory currents into the cortical cells. We study a network model with excitatory and inhibitory populations of simple binary units. The internal feedback is mediated by relatively large synaptic strengths, so that the magnitude of the total excitatory as well as inhibitory feedback is much larger than the neuronal threshold. The connectivity is random and sparse. The mean number of connections per unit is large but small compared to the total number of cells in the network. The network also receives a large, temporally regular input from external sources. An analytical solution of the mean-field theory of this model which is exact in the limit of large network size is presented. This theory reveals a new cooperative stationary state of large networks, which we term a balanced state. In this state, a balance between the excitatory and inhibitory inputs emerges dynamically for a wide range of parameters, resulting in a net input whose temporal fluctuations are of the same order as its mean. The internal synaptic inputs act as a strong negative feedback, which linearizes the population responses to the external drive despite the strong nonlinearity of the individual cells. This feedback also greatly stabilizes the system's state and enables it to track a time-dependent input on time scales much shorter than the time constant of a single cell. The spatio-temporal statistics of the balanced state is calculated. It is shown that the auto-correlations decay on a short time scale yielding an approximate Poissonian temporal statistics. The activity levels of single cells are broadly distributed and their distribution exhibits a skewed shape with a long power-law tail. The chaotic nature of the balanced state is revealed by showing that the evolution of the microscopic state of the network is extremely sensitive to to small deviations in its initial conditions. The balanced state generated by the sparse strong connections is an asynchronous chaotic state. It is accompanied by weak spatial cross-correlations, the strength of which vanishes in the limit of large network size. This is in contrast to the synchronized chaotic states exhibited by more conventional network models with high connectivity of weak synapses.

1 Introduction

The firing patterns of neurons in the cortex of intact animals often exhibit a strong degree of temporal irregularity. This can be seen by the broad Inter-Spike-Interval Histogram (ISI) of cortical neurons which are typically close to those generated by a Poisson process with a short refractory period (Abeles, 1991, Bair *et al.* 1994, Burns and Webb 1976, Douglas *et al.* 1991, Softky and Koch 1993). The irregular neuronal dynamics is also manifested in intracellular recordings of the membrane potential which exhibit strong temporal fluctuations. One of the long standing problems in cortical dynamics is understanding the origin of this irregularity and its computational implications (Douglas and Martin 1991, Ferster and Jagadeesh 1992). *In vitro* experiments show that cortical neurons fire in a relatively regular fashion when they are injected with a constant current. Thus the irregularity of the *in vivo* neuronal activity must be due to fluctuations in their synaptic input (Holt *et al.* 1996, Mainen and Sejnowski 1995). These fluctuations may be due to variations in the intensity of the sensory stimuli or may result from the stochastic action of synapses. However, since cortical cells have thousands of synaptic contacts, one would expect that the summation of the synaptic inputs at the soma averages out most of the fluctuations in the synaptic input and yields a membrane potential with only a small residual fluctuation. This is a particularly difficult issue in conditions where the cortex is vigorously active so that the cell receives many synaptic inputs within a single integration time constant (Holt *et al.* 1996, Softky and Koch 1993). One possible resolution of this problem is to assume that the fluctuating synaptic inputs are substantially correlated and therefore are not averaged out. Indeed, the spike trains of pairs of neurons in cortex and in thalamus are often correlated in a relatively narrow time scale (of the order of $10\,msec$) (Abeles 1991, Gray and Singer 1989, Perkel *et al.* 1967a,b, Vaadia *et al.* 1995). However, the observed size of these correlations indicates that in general only a small fraction of the neuronal activity is tightly correlated. Another possibility, which is addressed in this paper, is that although the inputs to a cell are only weakly correlated, the cell is sensitive to the residual correlations in the somatic potential.

Several mechanisms that generate enhanced sensitivity of a cell to small fluctuations in its potential have been explored (Bell *et al.* 1994, Ermentrout and Gutkin 1996, Gerstein and Mandelbrot 1964, Shadlen and Newsome 1994,1995, Softky 1995, Troyer and Miller 1996). One possibility is that the excitatory and inhibitory inputs to a cortical cell are balanced in such a way that leaves the cell's average potential close to threshold and its firing pattern is therefore susceptible to small fluctuations. An interesting question then is what might be the mechanism that leads to this balance. An interesting recent study (Tsodyks and Sejnowski 1995) explored the possible involvement of local cortical dynamics in balancing excitation and inhibition. This numerical study invoked a strong stochasticity in the synaptic action in the form of a large failure probability. In a related study (Amit and Brunel 1996a,b), the variability in the network activity is at least partially due to fluctuating external inputs to the local network. In addition, both studies do not properly address important issues concerning the behavior of the models and the robustness of their variability as the network size is scaled-up.

In this paper we investigate the hypothesis that the *intrinsic deterministic* dynamics of local cortical networks is sufficient to generate strong variability in the neuronal firing patterns. Neuronal dynamics is highly non-linear, hence it may seem natural to expect that neuronal networks with deterministic dynamics will exhibit chaotic behavior. However, studies of simple models of large networks with a high degree of connectivity (Abbott and Van Vreeswijk 1993, Gerstner and Van Hemmen 1993, Grannan *et al.* 1992, Hansel *et al.* 1995, Van Vreeswijk 1996, Wilson and Cowan 1972) reveal that in the absence of external sources of strong stochastic noise they tend to settle into temporally ordered states of tonic firing or oscillations. Recent extensive numerical study (Bush and Douglas 1991, Hansel and Sompolinsky 1992,1996) of a model of local circuits in visual cortex with realistic conductance-based dynamics has shown the existence of parameter regimes in which these networks exhibit strongly irregular states, denoted as *synchronized chaotic* states. These chaotic states are generated by the emergence of strong synchrony in the fluctuating activity of different neurons, which in turns generates self-consistently a strong fluctuating feedback to each cell. Thus, this is a network realization of the scenario of correlated synaptic inputs, mentioned above. The resulted patterns of activity show strongly synchronized bursting patterns, tightly timed by the common inhibitory feedback. While bursting patterns are sometimes observed in cortical networks, these *synchronized chaotic* states are hard to reconcile with the Poisson-like weakly correlated firing patterns, as is commonly observed in cortex.

In this work we explore the possibility that local networks with intrinsic dynamics evolve towards states that are characterized by strong chaos in conjunction with weak cross-correlations, through the mechanism of balancing between excitation and inhibition. This possibility raises several questions: (I) What are the conditions under which a network evolves to a state in which the excitatory and inhibitory inputs are balanced. (II) What are the characteristics of this balanced state? Does the balanced state represent a cooperative state which is qualitatively distinct from the synchronized chaotic state? (III) What are the functional advantages of the balanced state?

We study the above questions using a network model with the simplified dynamics of binary elements. The architecture consists of excitatory and inhibitory populations connected by sparse random connections. An essential ingredient of our model is the introduction of strong connections among the units. A cell is connected, on the average, to K other cells and K is large. However, the gap between the threshold of the cell and its resting potential is only of the order of $\sqrt{K}$ excitatory inputs. Thus the network will saturate unless a dynamically developed balance between the excitatory inputs and the inhibitory inputs to a cell emerges. Indeed, our analytical solution of the model in the limit of large network size shows that in a broad range of parameters the network settles into a stable balanced state. An interesting feature of the present theory is that it goes far beyond calculating the properties of the macroscopic order parameters. The theory yields a complete statistical characterization of the balanced state. It shows that the balanced state is associated with a strong Poisson-like firing pattern and also with a broad inhomogeneity in the average rates of individual neurons. Finally, we address the possible functional implications of the balanced state by showing that the network is capable of *fast tracking* of temporal changes in the external input to the network.

The outline of the paper is as follows: In Section 2 we present the model's dynamics and architecture. Section 3 presents the mean-field dynamic equations of the evolution in time of the two macroscopic order parameters which are the rates of activity of the two subpopulations. The mean-field theory is exact in the limit of large network size, N, and $1 \ll K \ll N$. In Section 4 the behavior of the population rates in the balanced state is studied. Section 5 is devoted to the spatial and temporal distribution of activity within the network. Section 6 addresses the stability of the balanced state. It shows that there is a comfortable parameter regime where the balanced state is stable. We also discuss what happens to the network when the balanced fixed-point is unstable. Section 7 considers the effect of inhomogeneity in the local thresholds. We show that in the presence of inhomogeneity the distribution of rates acquires a characteristic skewed shape with a long tail, qualitatively similar to the observed distribution of rates in populations of neurons in the cortex of behaving monkeys. In Section 8, we evaluate the sensitivity of the temporal fluctuations in the local instantaneous activities to a small change in the initial condition. We conclude that a small change in the initial condition leads rapidly to a complete loss of memory of the unperturbered initial conditions. Thus, our network shows the main characteristics of chaotic systems. Section 9 studies the dynamic response of the system to dynamic changes in the external input, and shows the fast tracking capabilities of the network. In Section 10 we discuss the results and some open issues. Details of the theory are outlined in Appendix A and B.

A preliminary report on this work was published in Van Vreeswijk and Sompolinsky (1996).

2 The Model

We consider a network of N_1 excitatory and N_2 inhibitory neurons. The network also receives input from excitatory neurons outside of the network

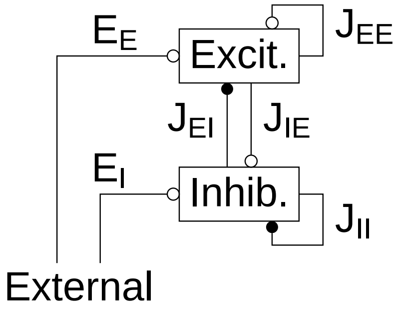

Figure 1: A schematic representation of the network architecture. Excitatory connections are shown as open circles, inhibitory ones as filled circles.

(see Fig. 1). We will use either the subscript 1 or E to denote the excitatory population and 2 or I for the inhibitory one. The pattern of connections is random but fixed in time. The connection between the i-th postsynaptic neuron of the k-th population and the j-th presynaptic neuron of the l-th population, denoted J_{kl}^{ij}, is $J_{kl}/\sqrt{K}$ with probability K/N_k and zero otherwise. Here $k, l = 1, 2$. The synaptic constants J_{k1} are positive and J_{k2} negative. Thus, on average, K excitatory and K inhibitory neurons project to each neuron. We will call K the connectivity index. The state of each neuron is described by a binary variable σ. The value $\sigma = 0$ ($\sigma = 1$) corresponds to a quiescent (active) state. The network has an asynchronous dynamics where only one neuron updates it state at any given time. The updated state of the updating neuron at time t is

$$\sigma_k^i(t) = \Theta(u_k^i(t)) \tag{2.1}$$

where $\Theta(x)$ is the Heaviside function, $\Theta(x) = 0$ for $x \leq 0$ and $\Theta(x) = 1$ for $x > 0$. The total synaptic input, u_k^i to the neuron, relative to the threshold, θ_k, at time t is

$$u_k^i(t) \;=\; \sum_{l=1}^{2} \sum_{j=1}^{N_l} J_{kl}^{ij} \sigma_l^j(t) + u_k^0 - \theta_k. \tag{2.2}$$

where u_k^0 denotes the constant external input to the k-th population. As explained in Appendix B the precise definition of the order of updates is not essential. One model is a stochastic model in which each neuron updates its state at time intervals which have Poisson statistics. This model is the simplest to analyze. However, it has the drawback that it introduces a stochastic element (the random choice of the updating neuron). An alternative model is a fully deterministic one in which each neuron updates its state at equally spaced times where the time between updates is different for each neuron. We show in Appendix B that the two models have the same mean-field equations. In both cases, the mean intervals between consecutive updates of a neuron of the k-th population is τ_k. We will use time units such that $\tau_E = 1$ so that the only independent time parameter is $\tau \equiv \tau_I$.

To make correspondence with point processes we define a spike as the transition from the passive (0) to the active (1) state. Note that the firing rate, r_k^i, of neuron i in population k is different from the the average value, $m_k^i(t)$, of σ_k^i because, before the cell can spike, it first has to update to the passive state. However if neuron i of the kth population updates to the active state in two consecutive updates, the synapses projecting from this cell stay active after the second update, even though no new spike is emitted. However if m_k^i, which we will call the activity rate, is small, the probability of two consecutive updates to the active state is low, and thus for small m_k^i, the activity rate and the firing rate are nearly equal. Indeed if we assume that at each update the probability of being in the active state is m_k^i (which is very nearly true in this model for low rates as shown in section 5.3), the firing rate is given by $r_k^i = m_k^i(1 - m_k^i)/\tau_k$.

An central ingredient of our model is the assumption that the total excitatory feedback current and the total inhibitory current into a cell are large compared to the neuronal threshold. We model this by choosing thresholds θ_k that are of order 1 and by assuming that the strength of individual synapses is of order $1/\sqrt{K}$, *i.e.*, the coefficients J_{kl} are of order unity. Furthermore, as will be seen later it is crucial that the excitatory inputs from the external sources too are large compared to the threshold. This is modeled by denoting these inputs as

$$u_k^0 = E_k\, m_0 \sqrt{K} \quad k = 1, 2 \tag{2.3}$$

where E_k is of order unity and $0 < m_0 < 1$ represents the mean activity of the external neurons. We will also use the notation

$$E_1 = E \tag{2.4}$$

for the external input to the excitatory population and

$$E_2 = I \tag{2.5}$$

for the external input to the inhibitory neurons. As noted above we assume that the external input is temporally regular.

Since the model neurons are threshold elements, the absolute scale of u_i^k is irrelevant. We therefore set

$$J_{EE} = J_{IE} = 1 \tag{2.6}$$

so that the only connection parameters from the network are the inhibitory and external ones, which we will denote as

$$J_E \equiv -J_{EI} \quad ; J_I \equiv -J_{II} \tag{2.7}$$

where $J_I, J_E > 0$.

3 Mean-Field Equations for Population Rates

The dynamics of our model can be described by mean-field theory, which is exact in the limit of large N_k. To define this limit we will assume that N_I/N_E is held fixed as the network size $N = N_E + N_I$ grows. The nature of the mean-field theory depends on the assumed relationship between the network size and the connectivity index. Conventional mean-field theory assumes that the networks are *fully connected*, which is defined here to mean that K/N is fixed as $N \to \infty$. Here we assume *sparse connectivity* defined by assuming that K fixed as N grows. As explained in the Introduction, we are primarily interested in temporal variability that is present in highly connected networks. *Highly connected* networks are either fully connected or sparsely connected with large connectivity index. Therefore we will focus on the case of large K. Technically, we will first take the limit $N \to \infty$ and then the limit $K \to \infty$. In reality, networks have a large fixed size and connectivity so that the distinction between full and sparse connectivity may be problematic. Nevertheless, roughly speaking, the sparse limit is appropriate as long as

$$1 \ll K \ll N_k \ , \quad k = 1, 2. \tag{3.1}$$

The mean-field theory of our model for arbitrary fixed K is presented in Appendix A. Taking the large K limit provides a substantial simplification of the mean-field equations. In this limit most of the properties of the system can be expressed in terms of the first and second moments of the neuronal activity lavels as will be shown here and in the following sections. We first consider the population-averaged firing rates of the excitatory and inhibitory cells as

$$m_k(t) = [\sigma_k^i(t)] = \frac{1}{N_k} \sum_{i=1}^{N_k} \sigma_k^i(t) \quad , \quad k = 1, 2 \tag{3.2}$$

where [...] denotes a population average. In Appendix A we show that the average activities satisfy in the large K limit

$$\tau_k \frac{d}{dt} m_k(t) \; = \; -m_k(t) \; + \; H\left(\frac{-u_k}{\sqrt{\alpha_k}}\right) \tag{3.3}$$

Here H is the complementary error-function

$$H(z) \equiv \int_z^\infty \frac{dx}{\sqrt{2\pi}} e^{-x^2/2} \; . \tag{3.4}$$

shown in Fig. 2. the quantities $u_k(t)$ and $\alpha_k(t)$ are

$$u_k(t) = \sqrt{K} \left(\sum_{l=1}^{2} J_{kl}\, m_l(t) + E_k\, m_0 \right) - \theta_k \tag{3.5}$$

and

$$\alpha_k(t) = \sum_{l=1}^{2} (J_{kl})^2\, m_l(t) \; , \tag{3.6}$$

respectively. Equation (3.5) denotes the population-average of the total input to a neuron in the k-th population, relative to threshold. Equation (3.6) denotes the variance of this input. Note that the external population does not contribute to variance because we assumed that the input is the same for all the neurons in a population.

In the case of a constant external input, namely, $m_0(t) = m_0$, the network settles into a state in which the average activities are constant, $m_k(t) = m_k$, given by the stable fixed-points of Eq. (3.3),

$$m_k \; = \; H\left(\frac{-u_k}{\sqrt{\alpha_k}}\right) \tag{3.7}$$

where the mean inputs are

$$u_E = (Em_0 + m_E - J_E m_I)\sqrt{K} - \theta_E, \tag{3.8}$$

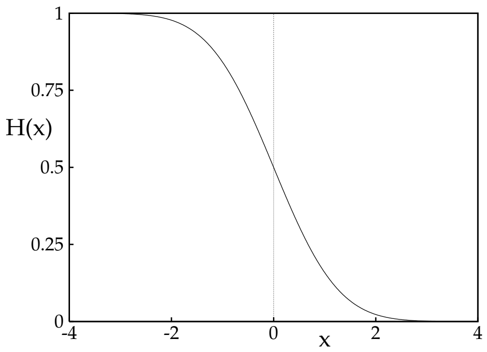

Figure 2: Complementary error function $H(x)$. The error function varies sigmoidally from 1 for $x \to -\infty$, to 0 at $x \to \infty$.

$$u_I = (Im_0 + m_E - J_I m_I)\sqrt{K} - \theta_I. \tag{3.9}$$

The variance of the inputs is

$$\alpha_k \; = \; m_E + J_k^2 m_I. \tag{3.10}$$

Equation (3.3) reflects the fact that the instantaneous input to each neuron $u_i^k(t)$ fluctuates across the population of neurons, and these fluctuations obey a Gaussian statistics in the large K limit. The expressions for the mean and variance of the input to a cell can be derived in the large K limit, by the following arguments. The population average inputs is

$$u_k(t) \; = \; [u_k^i(t)] = \sum_{l=1}^{2} \sum_{j=1}^{N_l} [\, J_{kl}^{ij} \,] \, [\, \sigma_l^j(t) \,] \; + u_k^0 - \theta_k \tag{3.11}$$

The population average $[J_{kl}^{ij}]$ is equivalent to quenched average over the random connectivity and is therefore equal to $J_{kl}\sqrt{K}/N$, yielding Eq. (3.5). Note that in the right hand side (RHS) of Eq. (3.11) we have neglected the correlations between the random fluctuations in the activity of a cell and the particular realization of its *output* connectivity. This is justified since such correlations are weak in the large N limit. Similarly, the variance α_k of the input is

$$\alpha_k(t) = [(\delta u_k^i(t))^2] = \sum_{l,l'=1}^{2} \sum_{j,j'=1}^{N_l} [\, (\, \delta(J_{kl}^{ij} \, \sigma_l^j(t)) \,)^2 \,] \tag{3.12}$$

where $\delta X \equiv X - [X]$. Observing that $[(J_{kl}^{ij} \, \sigma_l^j(t))^2] = J_{kl}^2 m_l/N$ whereas $[(J_{kl}^{ij} \, \sigma_l^j(t))]^2 = J_{kl}^2 m_l^2 K/N^2$ which is negligible, one obtains Eq. (3.6).

4 Population Rates in the Balanced State

The balanced state is characterized as a state in which the temporal fluctuations in the inputs are of the same order as the distance between the mean input relative to threshold (even when K is large). To show this we need to probe directly the network temporal properties. Here we study the necessary consequences of the balanced state on the behavior of the population rates. A necessary condition for a balanced state is that both the excitatory and the inhibitory populations do not fire at their maximum rate, or are completely silent, when we take the limit $K \to \infty$. In other words we look for solutions with $0 < m_k < 1$ in the large K limit.

To have equilibrium rates with $m_k \neq 0, 1$ in the large K limit, both u_E and u_I have to be finite in this limit. This means that the RHS of Eqs. (3.8)-(3.9) vanish to leading order. This leads to the following equations

$$Em_0 + m_E - J_E m_I = O(1/\sqrt{K}) \tag{4.1}$$

$$Im_0 + m_E - J_I m_I = O(1/\sqrt{K}) \tag{4.2}$$

Thus, in the large K limit we obtain

$$m_E = \frac{J_I E - J_E I}{J_E - J_I} m_0 \equiv A_E m_0. \tag{4.3}$$

$$m_I = \frac{E - I}{J_E - J_I} m_0 \equiv A_I m_0, \tag{4.4}$$

Since both A_E and A_I have to be positive the coupling strengths have to satisfy

$$\frac{E}{I} > \frac{J_E}{J_I} > 1 \tag{4.5}$$

or

$$\frac{E}{I} < \frac{J_E}{J_I} < 1. \tag{4.6}$$

Besides this balanced solution we should also examine the possibility of unbalanced solutions in which either $m_k = 0$ and u_k is of order $\sqrt{K}$ and negative or, $m_k = 1$ and u_k is of order $\sqrt{K}$ and positive. Equation (4.6) admits an unbalanced solution in which $m_E = 0$. In this solution m_I is to leading order given by $m_I = Im_0/J_I$ (since the leading order in u_I should vanish) so that

$$u_E = \sqrt{K}(E - J_E I/J_I) m_0 < 0. \tag{4.7}$$

Furthermore if $J_E < 1$ and $J_I < 1$ there exists a solution with $m_E = m_I = 1$ even for $m_0 = 0$. In this solution u_k satisfies to leading order

$$u_k = \sqrt{K}(1 - J_k) \quad (k = E, I). \tag{4.8}$$

So u_k is of order $\sqrt{K}$ and positive.

Thus if we require that there be no stationary solutions with $m_E = 0, 1$ or $m_I = 0, 1$ for small m_0, the following constraints have to be satisfied

$$\frac{E}{I} > \frac{J_E}{J_I} > 1 \tag{4.9}$$

$$J_E > 1. \tag{4.10}$$

It is straightforward to show that these constraints eliminate all possible unbalanced states.

Throughout the paper we will assume that Eqs. (4.9) and (4.10) are satisfied, and that m_0 is small enough, so that $A_k m_0 < 1$. Equations (4.3)-(4.4) imply that the network activity rates grow linearly with the external rate, $m_k = A_k m_0$, even though microscopic dynamics is highly nonlinear. This is because the network dynamically finds an operating point at which the net input in both populations is balanced. Thus, the linearity in the network rates reflects the linearity of the synaptic summation underlying our model.

4.1 The Net Input

The above equations determine the average rates of the populations, but they must be consistent also with the general equilibrium results Eq. (3.7). According to Eqs. (4.3) and (4.4) the leading $O(\sqrt{K})$ contributions to u_k cancel each other. Thus, the net value of u_k is determined by subleading contributions, such as corrections of order $1/\sqrt{K}$ to m_k. In fact, Eq. (3.7) should be viewed as equations that *determine* the net synaptic inputs u_k given the mean activity rates m_k, Eqs. (4.3)-(4.4). It is useful to denote by $h(m)$ the scaled input of m, defined as the solution of the equation

$$m = H(-h) \tag{4.11}$$

Thus Eq. (3.7) reduces to

$$u_k = \sqrt{\alpha_k} h(m_k). \tag{4.12}$$

The activity of neurons in cortex is usually much less than the saturation rate. It is therefore useful to consider the limit where $m_0 \ll 1$. In this regime $m_k \ll 1$ and we can use the approximation

$$H(x) \approx \frac{\exp(-x^2/2)}{\sqrt{2\pi}|x|} \tag{4.13}$$

to obtain

$$h(m) \approx -\sqrt{2|\log m|} \tag{4.14}$$

Substituting this result in Eq. (4.12) yields

$$u_k \approx -\sqrt{2\,\alpha_k|\log \alpha_k|} \tag{4.15}$$

This relation between m_k and u_k will be needed below in the calculation of the rate distribution (Section 5.1).

4.2 Finite K Corrections

For finite K the residuals of order $1/\sqrt{K}$ in the rates are not negligible so that Eqs. (4.3) and (4.4) no longer hold exactly. For finite K the equilibrium activities satisfy $m_k = F_k(m_E, m_I)$, with F_k given be Eq. (A.5). However, as long as

$$m_k \gg K^{-1} \tag{4.16}$$

the Gaussian assumption of the input statistics is a good approximation, hence Eqs. (3.7) still hold. Thus, the leading finite K corrections can be incorporated by resorting to the full mean-field equations Eqs. (3.3)-(3.10). In particular, the finite K equations for the fixed-point are

$$Em_0 + m_E - J_E m_I = (\theta_E + \sqrt{\alpha_E}h(m_E))/\sqrt{K} \tag{4.17}$$

$$Im_0 + m_E - J_I m_I = (\theta_I + \sqrt{\alpha_I}h(m_I))/\sqrt{K}. \tag{4.18}$$

As long as m_0 is not small, the right hand sides of these equations are small for large K hence the corrections to the linear solution, Eqs. (4.3)- (4.4) are small. When m_0 becomes sufficiently small (*i.e,* of order $1/\sqrt{K}$ or less) the strong non-linearity in the single neuron dynamics reveals itself in a strong non-linearity in the population response. In particular, the effect of the single neuron threshold θ_k becomes important. This is seen in Fig. 3 where the

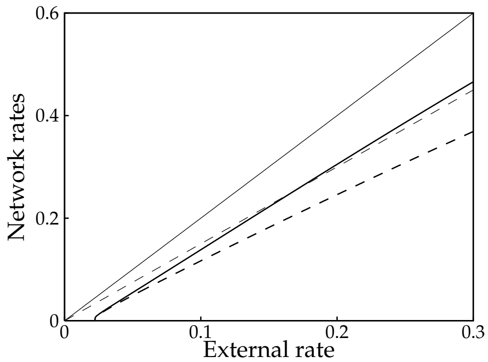

Figure 3: The mean activity of the excitatory population (thick solid line) and the inhibitory population (thick dashed line) as a function of the input activity. For a network in which cells receive input from, on average, 1000 cells in each population. For comparison the activities in the large K limit are also shown, (thin solid line for the excitatory and thin dashed line for the inhibitory population respectively). Parameter values: $E = 1$, $I = 0.8$, $J_E = 2$, $J_I = 1.8$, $\theta_E = 1$ and $\theta_I = 0.7$.

population rates are evaluated by the finite K equations, Eqs. (4.17)-(4.18) with $K = 1000$. For comparison, we also show the straight lines predicted by the large K limit. Since, as mentioned above, the steady state rates in cortical networks are usually low, it is sometimes useful to incorporate the leading finite K corrections. Whenever we refer in subsequent figures explicit values for K we use Eqs. (4.17)-(4.18), unless otherwise stated. Except for thresholding the population rates, the finite K corrections affect only the quantitative results but not the qualitative predictions of the simple large K theory.

5 Spatial and Temporal Variability

So far we have been concerned only with the population average rates m_k. However the fact that the population averages are not saturated does not necessarily imply that the system's state exhibits strong temporal variations. Specifically, a population average excitatory rate m_k, may be the outcome of a fluctuating state where all the cells in the k-th population fire a fraction m_k of the time. However, it can also be achieved by a frozen state in which a fraction m_k of the cells fire every time these cells are updated, while all other cells never fire. In other words, the population average does not distinguish between temporal and spatial fluctuations of activity levels.

Fortunately, the mean-field theory fully characterizes the statistics of both the spatial and the temporal fluctuations in the activities in the balanced state. This statistics can be expressed by writing the instantaneous activity of a cell as threshold function of two random variables x_i and $y_i(t)$,

$$\sigma_k^i(t) = \Theta\left(-u_k + \sqrt{\beta_k}\, x_i + \sqrt{\alpha_k - \beta_k}\, y_i(t)\right) \tag{5.1}$$

The means u_k are given by Eqs. (3.8)-(3.9). The parameter β_k is given by

$$\beta_k = q_E + J_k^2 q_I \tag{5.2}$$

The order parameter q_k is defined as

$$q_k = \frac{1}{N_k} \sum_{i=1}^{N_k} (m_k^i)^2. \tag{5.3}$$

where m_k^i is the time-averaged activity rate of the i-th cell,

$$m_k^i \equiv < \sigma_k^i(t) > \tag{5.4}$$

The symbol $< ... >$ denotes average over long time. Both x_i and $y_i(t)$ are independent Gaussian variables with zero mean and unit variance.

Quenched Fluctuations of Synaptic Inputs: The term proportional to x_i represents a quenched random component of the synaptic input received by different cells and thus represents a spatial inhomogeneity in the rates. The origin of this inhomogeneity is two-fold. Since in our model the connectivity is random, cells may differ in the *number* of synaptic inputs they have. This component is given by

$$\delta_1 < u_k^i > = \sum_{l=1}^{2} \sum_{j=1}^{N_l} \delta J_{kl}^{ij}\, [m_l^j]. \tag{5.5}$$

Here $\delta J_{kl}^{ij} = J_{kl}^{ij} - [J_{kl}^{ij}]$. In addition, different neurons are connected to different cells so that even if all the cells would have received the same number of inputs the system would evolve into a state with a self-consistently developed spatial inhomogeneity. The second component can be written as

$$\delta_2 < u_k^i >= \sum_{l=1}^{2} \sum_{j=1}^{N_l} J_{kl}^{ij} \, \delta m_l^j \tag{5.6}$$

where $\delta m_l^i \equiv m_l^i - m_l$. Adding the two contributions yields

$$[\,(\delta < u_k^i(t) >)^2] = \sum_{l=1}^{2} J_{kl}^2 q_l = q_E + J_k^2 q_I = \beta_k \tag{5.7}$$

Thus, this variance represents the fluctuation in both the number and the identity of input cells to the different cells.

Temporal Fluctuations of Synaptic Inputs: The term in eq. (5.1) which is proportional to $y_i(t)$ represents the stochastic component of the inputs to a cell, namely a temporally fluctuating component which has a short-time correlations. This can be written as

$$u_k^i(t) - < u_k^i > = \sum_{l=1}^{2} \sum_{j=1}^{N_l} J_{kl}^{ij} \, (\sigma_k^j(t) - m_k^j) \tag{5.8}$$

from which one obtains

$$[\,(u_k^i(t) - < u_k^i >)^2] \; = \; \sum_{l=1}^{2} J_{kl}^2 (m_l - q_l) = m_E - q_E + J_k^2 (m_I - q_I) = \alpha_k - \beta_k \tag{5.9}$$

Note that the variance of the temporal fluctuations in the inputs depends on $m_k - q_k$ which in turn measures the temporal variability of the state.

5.1 Distribution of Time-Averaged Rates

The distribution of rates in the k-th population is defined as

$$\rho_k(m) \equiv N_k^{-1} \sum_{i=1}^{N_k} \delta(m - m_i^k) \tag{5.10}$$

The statistics of the time average local rates can be derived by averaging Eq. (5.1) over $y_i(t)$ (which is equivalent to average over time),

$$m_k^i = m_k(x_i) = H\left(\frac{-u_k + \sqrt{\beta_k}\, x_i}{\sqrt{\alpha_k - \beta_k}}\right) \quad . \tag{5.11}$$

Thus, the distribution of m_k^i is fully determined by its first two moments. Averaging this equation over x_i yields Eq. (3.7). Similarly, squaring Eq. (5.11) and averaging over x_i yields

$$q_k = \int Dx \left[H\left(\frac{-u_k + \sqrt{\beta_k}\, x}{\sqrt{\alpha_k - \beta_k}}\right)\right]^2 . \tag{5.12}$$

Here we have used the Gaussian measure $Dx \equiv dx \exp(-x^2/2)/\sqrt{2\pi}$. In general, q_k satisfies $(m_k)^2 \leq q_k \leq m_k$. The smaller q_k, the more homogeneous the rate distribution. In a frozen state in which a fraction m_k of the cells are active every time they are updated, while all other cells are always quiescent, q_k is given by $q_k = m_k$. On the other hand, if all cells in the population have a probability m_k of being active each time they are updated, $m_i^k = m_k$, $q_k = (m_k)^2$. Equations (5.12) have two solutions. There is a solution with $q_k = m_k$, corresponding to a frozen state, but this solution is unstable. The stable solution has $(m_k)^2 < q_k < m_k$, which corresponds to a temporally fluctuating state. Although the frozen solution is an unstable one–as mentioned above–its existence highlights the fact that the temporal variability in our system is purely of deterministic origin and is not induced by external stochastic sources.

Generalizing Eq. (5.12), we can write

$$\rho_k(m) = \int Dx\, \delta(m - m_k(x)) \tag{5.13}$$

In Appendix A.1 we analyze the properties of this distribution. A numerical evaluation of $\rho_k(m)$ is shown in Fig. 4 which displays the rate distribution of the excitatory activity for different values of m_E. The distribution is plotted against m/m_E. The synaptic couplings were kept constant, while the mean rates were varied by adjusting the external rate m_0. For high mean activity levels the distribution has a pronounced skewed shape. Note however that according to Eq. (5.11) the distribution of the time average *inputs* u_i^k to the cells is Gaussian, for all values of m_k.

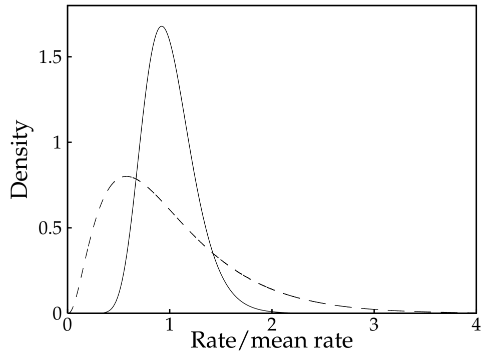

Figure 4: Distribution of the activity rates of the excitatory population for two different values of the average rate in the large K limit: $m_E = 0.01$ (solid line), and $m_E = 0.1$ (dashed line). The distributions are shown as a function of the local rate divided by the mean rate. Parameter values as in Fig. 3.

In the low rate limit, $m_0 \ll 1$, Eq. (5.12) can be solved using Eqs. (4.13)-(4.15) yielding to leading order,

$$q_k = m_k^2 + O(m_k^3 |\log m_k|). \tag{5.14}$$

Thus, if the network evolves to a state with low average activity levels, $m_k \ll 1$, q_k is slightly larger than m_k^2. The fact that $q_k \ll m_k$ implies that the balanced state is characterized by strong temporal fluctuations in the activity of the individual cells. On the other hand, the fact that q_k is not exactly equal to m_k^2, reflects the spatial inhomogeneity in the time-averaged rates within a population, as discussed above. Equation (5.14) implies that when the mean activity m_k decreases the width of the distribution is proportional to $(m_k)^{3/2}$, *i.e.,* it decreases faster than the mean m_k. Thus, for low mean activity, $\rho_k(m)$ becomes narrowly peaked at $m = m_k$, as shown in Fig. 4. The reason for the narrow peak is the fact that in our model the fluctuations in the input is related to the fluctuations in the feedback from the network, hence its variance becomes small as the activity in the network decreases (see Eq. (5.2).)

5.2 Time-Delayed Autocorrelations

In order to complete the statistical characterization of the balanced state we have to determine the statistics of the temporal fluctuations in the activities of single cells, or equivalently the temporal fluctuations in their input. We have already stated that the temporal fluctuations in $u_i^k(t)$ obey Gaussian statistics, with variance given by $\alpha_k - \beta_k$. To fully characterize its statistics we have to evaluate its auto-correlations. Using arguments similar to those outlined above, it is straightforward to show that the autocorrelation of the input is linearly related to the autocorrelations in the local activities,

$$\beta_k(\tau) = [< \delta u_i^k(t)\, \delta u_i^k(t+\tau) >] = q_E(\tau) + J_k^2 q_I(\tau) \tag{5.15}$$

where $q_k(\tau)$ is the time-delayed autocorrelations of the local activities,

$$q_k(\tau) = N_k^{-1} \sum_{i=1}^{N_k} < \sigma_i^k(t) \sigma_i^k(t+\tau) > \tag{5.16}$$

and as before $< ... >$ denotes average over t. Note that $q_k(0) = m_k$ whereas $q_k(\tau \to \infty) = q_k$. Likewise, $\beta_k(0) = \alpha_k$ whereas $\beta_k(\tau \to \infty) = \beta_k$. Using this relation, the following self-consistent equation for $q_k(\tau)$ (with $\tau \geq 0$) is obtained,

$$\begin{aligned} \tau_k \frac{dq_k(\tau)}{d\tau} &= -q_k(\tau) \\ &+ \int_0^\infty \frac{dt}{\tau_k} \exp(-t/\tau_k) \int Dx \left[H\left(\frac{-u_k - \sqrt{\beta_k(t+\tau)}\, x}{\sqrt{\alpha_k - \beta_k(t+\tau)}} \right) \right]^2 \end{aligned} \tag{5.17}$$

Note that the integral over t in Eq. (5.17) results from averaging over the distribution of update time intervals. The solution of this integral equation yields a function $q_k(t)$ which decays to its equilibrium value with a time constant of the order of τ_k. A numerical solution of Eq. (5.17) for $q_k(\tau)$ is shown in Fig. 5. As can be seen, the autocorrelations are larger than those predicted by Poisson statistics. This enhancement of short-time correlations reflect the refractoriness in the activities of the cells that project the cell.

5.3 Numerical Realization of Synaptic Inputs to a Cell

In order to demonstrate the nature of the fluctuating synaptic inputs to a single excitatory cell in the balanced state, we have generated numerically samples of stochastic Gaussian processes which simulates the fluctuations of

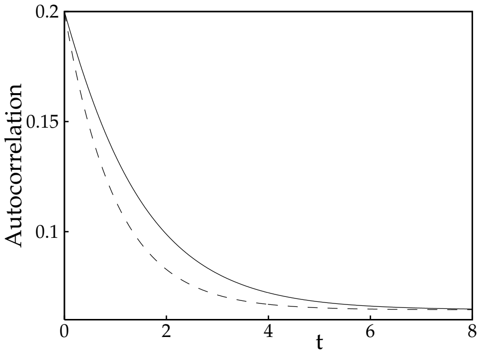

Figure 5: Population averaged autocorrelation for the excitatory population in the large K limit (solid line). The dashed line shows the autocorrelation for a population of cells with the same rate distribution, but Poissonian updating. Parameter values: $\tau = 0.9$, $m_0 = 0.1$, and other parameters as in Fig. 3.

the synaptic inputs to a single excitatory cell. In order to show explicitly the effect of balancing we have simulated separately the total excitatory and inhibitory components of $u^i_E(t)$. The time average of the total excitatory (inhibitory) component is itself sampled from a Gaussian distribution with a mean $\sqrt{K}(m_E + Em_0)$ ($\sqrt{K}J_E m_I$) , and a variance q_E ($J_E q_I$) . The time-dependent fluctuations of the total excitatory (inhibitory) input has a time-delayed auto-correlation equal to $q_E(\tau) - q_E$ ($J_E^2(q_I(\tau) - q_I)$). The results are shown in Fig. 6, where we have used $K = 1000$. They demonstrate that the total excitatory and inhibitory inputs are large compared to the threshold and have fluctuations that are small compared to their mean. Because the network is in the balanced state the net input is of the same order as the threshold and the fluctuations bring the input above threshold at irregular intervals. The lower part of the figure we show the output state of the cell. This is evaluated by generating the sequence of update times and thresholding the net input at these times. Note that, because of the update rule, the cell does not switch from passive to active every time the net input crosses the threshold.

In Fig. 7 we present the interspike interval histogram (ISI) of the cell. Note that because the interval between spikes is a convolution of two random events: first a transition from 1 to 0 and then a transition from 0 to 1, the ISI vanishes at small intervals. Thus, the above definition of a spike does capture

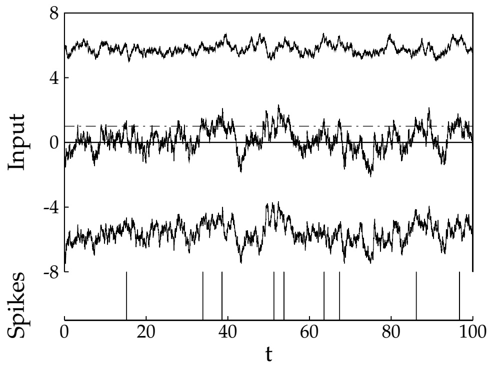

Figure 6: Temporal structure of the input to an excitatory cell. The upper panel shows the total excitatory input, consisting of the external input and the excitatory feedback (upper trace) the total inhibitory input (lower trace) as well as the net input (middle trace). They are calculated by sampling from the time-correlated Gaussian statistics predicted by the theory. Below the times when the cell switched to the active states are indicated. Parameter values: $m_0 = 0.04$ and other parameters as in Fig. 5. $K = 1000$ was used to calculate the average input.

to some extent the refractoriness of real spikes. In fact, if we ignore the short-time correlations in the activities, the ISI of the i-th (say, excitatory) cell with an average rate m_i can be shown to be simply

$$I_i(t) = \frac{m_i(1-m_i)}{\tau_E(1-2m_i)} \left(\exp(-m_i t/\tau_E) - \exp(-(1-m_i)t/\tau_E) \right) \quad , t \geq 0. \quad (5.18)$$

This function rises linearly from *zero* and peaks at $t \propto \tau_E$. For intervals of the order of τ_E/m_i or longer $I(t)$ decays purely exponentially with a decay constant m_i/τ_E as in the ISI of a single Poisson process with a rate m_i/τ_E. Comparison with Fig. 7 shows that this is indeed a very good approximation of the ISI of our model.

Finally, it should be noted that because of the sparsity of the connectivity different cells receive input from different sub-populations, so that the fluctuations in their input will be only very weakly correlated. As a result the correlations in their activity will have a very small correlation.

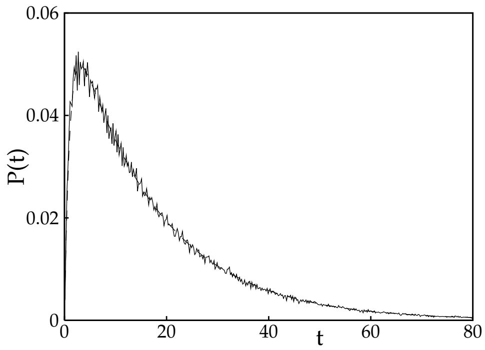

Figure 7: Interspike interval distribution for the cell shown in Fig. 5 (solid line). The distribution was determined by measuring the time between consecutive switches from the inactive to the active state until 5×10^5 intervals had been accumulated. The dashed line shows the interspike interval distribution for Poissonian updating with $m_i = 0.06$.

6 Stability of the Balanced State

To determine the stability of the balanced state we have to study the response of the system to small perturbations in the population activity rates. However, because of the nature of the balanced state, we have to distinguish two scales of perturbations: *local* perturbations in which the deviations in the rates are small compared to $1/\sqrt{K}$; and *global* perturbations in which these deviations are large compared to $1/\sqrt{K}$.

6.1 Local Stability

Local stability of the balanced state requires that a sufficiently small perturbation in the populations rates will decay to zero. In our case, a sufficiently small perturbation means that it initially causes only a small disruption of the balanced state. This means that the perturbations are small not only compared to m_k but also compared to $1/\sqrt{K}$ so that the perturbation of the inputs to the cells are initially small. We therefore consider a solution of Eqs. (3.3) with an initial condition $m_k(0) = m_k + \delta m_k(0)$ with a small $\delta m_k(0)$ where $|\delta m_k(0)| \ll 1/\sqrt{K}$. In this case the perturbation of the total mean input u_k is also small, hence we can linearize the dynamic equations (3.3) around their fixed point. Thus, $\delta m_k(t) = m_k(t) - m_k$ satisfy a linear equation of the form

$$\tau_k \frac{d}{dt}\delta m_k(t) \;=\; -\delta m_k(t) + \sqrt{K} \sum_{l=1,2} f_{kl}\delta m_l(t) \tag{6.1}$$

Calculating f_{kl} by partial differentiation of the RHS of Eq. (3.3), yields

$$f_{kl} = \frac{\exp(-u_k^2/2\alpha_k)J_{kl}}{\sqrt{2\pi\alpha_k}} \tag{6.2}$$

Solving Eqs. (6.1) one obtains $\delta m_k(t) = \delta m_{k,1}\exp(\lambda_1 t) + \delta m_{k,2}\exp(\lambda_2 t)$ where the eigenvalues λ_1 and λ_2 of the 2 by 2 equations Eqs. (6.1) are both of order $\sqrt{K}$. Requiring that their real part be negative yields a condition on τ of the form

$$\tau < \tau_L \tag{6.3}$$

where τ_L is of order 1, its precise value depends on the system parameters. It is important to note that since both λ_1 and λ_2 are of order $\sqrt{K}$, if $\tau < \tau_L$, small perturbations will decay with extremely short time constant of order $1/\sqrt{K}$. This is due to the strong negative feedback, of order $\sqrt{K}$, generated by the strong synaptic couplings.

6.2 Global Stability

The local stability condition Eq. (6.3) guarantees that a perturbation smaller than $O(1/\sqrt{K})$ will die out. It is therefore important to ask whether the balanced state is stable also to perturbations that are large compared to this order. However, such perturbation will generate a large disruption in the inputs u_k, of order $\sqrt{K}$, hence linearization of the dynamic equations is inadequate. We therefore have to consider the nonlinear evolution of perturbations in the rates under Eqs. (3.3). In fact, since the perturbation destroys the balance between excitation and inhibition, $H(-u_k/\sqrt{\alpha_k})$ of Eq. (3.3) can be approximated by $\Theta(u_k)$, hence the evolution of the perturbations is described by

$$\tau_k \frac{d}{dt}\delta m_k(t) \;=\; -\delta m_k(t) + \Theta(\delta m_E - J_k \delta m_I) - m_k. \tag{6.4}$$

These equations are piece-wise linear and therefore can be solved explicitly. One finds that the solution of these equations decay to zero provided that

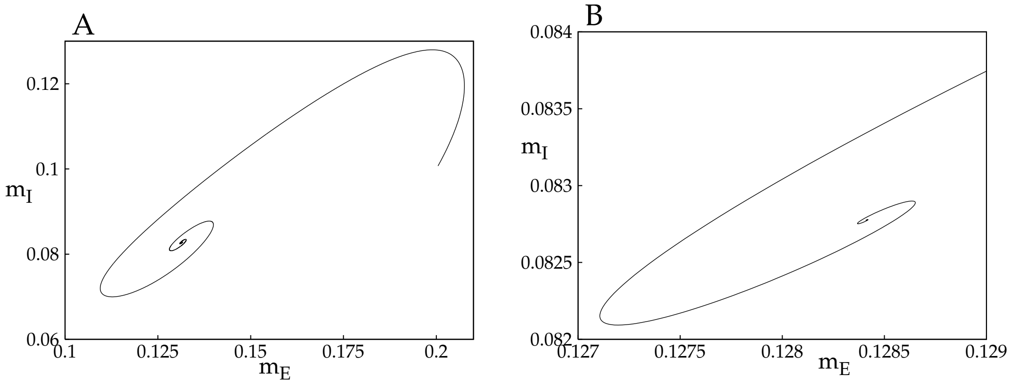

Figure 8: Evolution to the stable fixed point. The average inhibitory rate is plotted against the average excitatory rate. (A) shows the evolution of the rates when the rates are initialized far from their steady state values. (B) shows a close-up view of the approach to the fixed point. Parameters: $\tau = 1.3$. The other parameter values as in Fig. 3.

the inhibitory time constant satisfies

$$\tau < \tau_G \tag{6.5}$$

where

$$\tau_G = J_E \min \left\{ \sqrt{\frac{J_I m_I (1 - m_I)}{J_E m_E (1 - m_E)}}, \frac{m_I}{m_E}, \frac{1 - m_I}{1 - m_E} \right\} \tag{6.6}$$

In conclusion, the global stability condition guarantees that, starting from arbitrary initial values $m_k(0)$ the population rates will eventually approach the balanced regime characterized by local fields u_k which are of order 1 and not $\sqrt{K}$. In other words, the rates will deviate from the values of the balanced fixed point by at most $O(1/\sqrt{K})$ quantities. Whether they will actually approach this fixed point or will converge to a limit cycle around it depends on the local stability condition, Eq. (6.3). It should be pointed out that depending on the system parameters τ_G may be greater or smaller than τ_L. Figure 8 shows the evolution of m_E and m_I in a network with $K = 1000$, for $\tau = 1.3$, when the network starts far away from the balanced state. The initial evolution is similar to the global dynamics. It converges to the neighborhood of the balanced fixed point in an oscillatory manner characteristic of the dynamics of Eq. (6.4). In Fig. 8B we show the late portion of the dynamics which corresponds to the local dynamics, Eqs. (6.1).

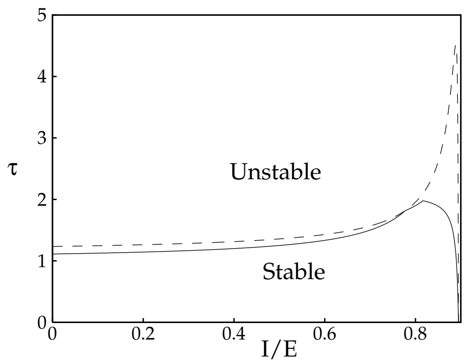

Figure 9: Critical time constants τ_G (solid line) and τ_L (dashed line) as function of I/E. The external rate was adjusted to keep the excitatory activity level constant at $m_E = 0.1$. I/E was varied from 0 to $(J_I - m_E)/(J_E - m_E)$. For this range of I/E, m_I varies from m_E/J_I to 1. Parameters: $E = 1$, $J_E = 2.0$, and $J_I = 1.8$.

For the parameters used in this Figure the large K critical inhibitory time constants are $\tau_L = 1.61$ and $\tau_G = 1.50$.

To illustrate the region of stability of the balanced state we have calculated the phase diagram of the network in terms of two parameters: The inhibitory time-constant τ, and the ratio between the external input into the inhibitory population, and the external input into the excitatory population. We have chosen to scale m_0 so that the excitatory population rate is held fixed. The results are shown in Fig. 9, where both the local and global stability lines are presented. Note that for these parameters τ_L is always smaller than τ_G.

6.3 Regimes of Instability

Stability of the balanced state requires that τ be smaller than both τ_L and τ_G. It is of interest to consider what happens if this condition is not fulfilled.

1. **Unbalanced Limit Cycle:** $\tau > max\{\tau_L, \tau_G\}$. In this case Eqs. (3.3) possess a stable unbalanced limit cycle, namely, a stable oscillatory solution with $u_k(t)$ of order $\sqrt{K}$. This is shown in Fig. 10A.

2. **Balanced Limit Cycle:** $\tau_L < \tau < \tau_G$ **.** In this case, perturbations that are of order 1 will decrease until they are of order $1/\sqrt{K}$, while

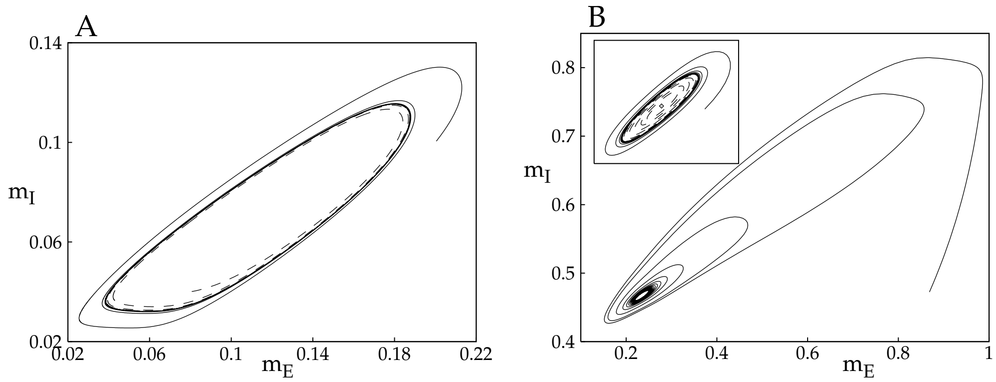

Figure 10: Different scenarios when the fixed point is unstable. (A) shows a case where τ is larger than both τ_G and τ_L. Here the rates evolve to the global limit cycle where the amplitude of the oscillations is of order 1. The solid line shows the evolution when the network is initiated outside the limit cycle, the dashed line corresponds to for initial rates inside the limit cycle. Parameters as in Fig. 8, except $\tau = 1.8$. (B) Shows schematically a case where $\tau_L < \tau < \tau_G$. The network evolves to a limit cycle with the amplitude of order $K^{-1/2}$. The figure shows the evolution of the rates with initial conditions far from the fixed point. The insert shows an expanded view of the area around the fixed point, with the trajectory of rates starting outside the limit cycle (solid line) and the trajectory of a network that was initiated close to the fixed point.

perturbations that are small compared to $1/\sqrt{K}$ will increase until they are of order $1/\sqrt{K}$. Since there are no fixed points with δm_k of order $1/\sqrt{K}$ this means that there has to be a stable limit cycle with an amplitude of order $1/\sqrt{K}$. Thus, in this regime the system converges to a limit cycle which maintains the approximate balance between excitation and inhibition. This is described schematically in Fig. 10B.

3. **Balanced Fixed-Point with Shrinking Basin: $\tau_G < \tau < \tau_L$.** In this case, perturbations of order 1 go to a global limit cycle, while perturbations much smaller than $1/\sqrt{K}$ evolve to the fixed point. There must be an unstable limit cycle with amplitude of order $1/\sqrt{K}$ that separates perturbations that go the global limit cycle and perturbations that go to the fixed point.

7 Inhomogeneous Thresholds

So far we have considered networks of identical neurons, except for their connectivity. Real neuronal systems exhibit a substantial inhomogeneity in single neuron properties. It is therefore important to consider how such inhomogeneities affect the behavior of our system. We will model the inhomogeneity by a variability in the thresholds of the neurons. Inhomogeneities in the local thresholds may have particularly strong effect in a balanced state with low mean activity. The reason for this is that the intrinsic fluctuations are all generated by feedback from the network activity. Hence they decrease in amplitude as the mean activity in the network drops. In particular, under these conditions the intrinsic temporal fluctuations may not be of sufficiently large amplitude to overcome the quenched dispersion of local thresholds. Therefore, the important issue which we address here is: does the balanced state remain temporally fluctuating in the limit of low mean activity in the presence of inhomogeneous thresholds, or does it become a frozen state. We will show that the answer to these questions depend not only on the width of the threshold distribution but also on the form of its tail.

We denote the local threshold of a neuron by $\theta_i^k + \theta_k$ where θ_k is the population averaged threshold and θ_i^k is a quenched random variable with zero mean. We will call θ_i^k the *local* threshold. The mean activity rate of neurons in the k-th population that have a local threshold θ is

$$m_k(\theta) = H\left(\frac{\theta - u_k}{\sqrt{\alpha_k}}\right). \tag{7.7}$$

and hence the population averaged rate is

$$m_k = \int d\theta P(\theta)\, H\left(\frac{\theta - u_k}{\sqrt{\alpha_k}}\right) \tag{7.8}$$

where $P(\theta)$ denotes the quenched distribution of θ, and u_k and α_k are given as before by Eqs. (3.8), (3.9), and (3.10). Note that we have absorbed the mean threshold, θ_k in the definition of u_k (see Eqs. (3.8)-(3.9)).

7.1 Distribution of Thresholds with Long Tails

We first consider a distribution with a long tail of low thresholds. A concrete example is

$$P(\theta) = \frac{1}{\Delta\sqrt{2\pi}} \exp(-\frac{1}{2}(\theta/\Delta)^2) \tag{7.9}$$

In this case, the spatial fluctuations in the inputs (relative to thresholds) consist of two Gaussian terms: one is induced by the random connectivity and has a variance α_k and the other induced by the thresholds and has a variance Δ. The balance conditions which determines the population rates, Eqs. (4.3)-(4.4), still holds. In addition,

$$m_k = H\left(\frac{-u_k}{\sqrt{\alpha_k + \Delta^2}}\right) \tag{7.10}$$

which determines u_k, and

$$q_k = \int Dx \left[H\left(\frac{-u_k - \sqrt{\Delta + \beta_k}\, x}{\sqrt{\alpha_k - \beta_k}}\right)\right]^2 \tag{7.11}$$

Now let us consider the limit of low mean rates, which is achieved by assuming that m_0 is small. For fixed Δ, if the mean rates become sufficiently low so that $m_k \ll \Delta$, the intrinsic variances α_k and β_k can be neglected compared with Δ, hence one obtains

$$m_k \approx q_k \approx H\left(\frac{-u_k}{\Delta}\right). \tag{7.12}$$

The fact that $q_k \approx m_k$ implies that the state is essentially a frozen state, namely,

$$m_k(\theta) \approx \Theta(u_k - \theta) \tag{7.13}$$

and consequently, the distribution of mean rates has a distinct bi-modal shape,

$$\rho_k(m) \approx (1 - m_k)\delta(m) + m_k\delta(m-1)\ , \quad m_k \ll 1 \tag{7.14}$$

as shown in Fig. 11A. Thus, an unbounded threshold distribution has a relatively strong qualitative effect on the balance state, in the limit of low mean rate.

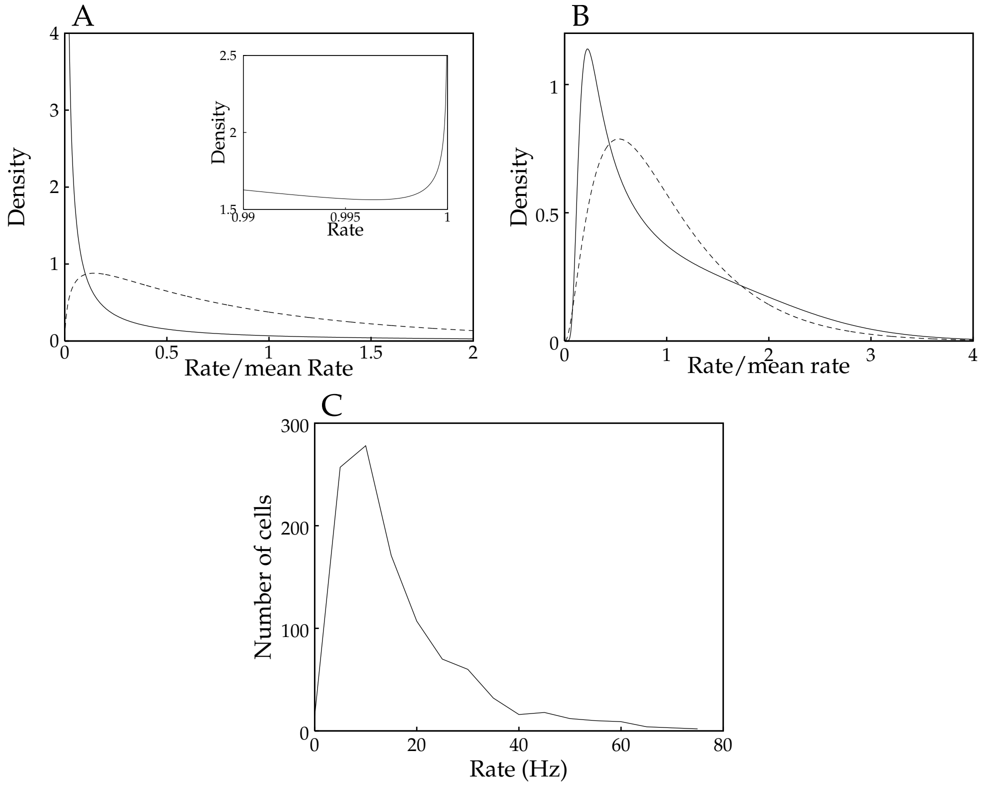

Figure 11: Distribution of the activities of the cells in the excitatory population in the large K limit. (A) Distribution for a network of neurons with a Gaussian distribution of thresholds. The distribution is shown for population averaged rates $m_E = 0.01$ (solid line) and $m_E = 0.1$ (dashed line). The insert shows the divergence at $m = 1$ of the distribution for $m_E = 0.01$ with the density in arbitrary units. Parameter values $D = 0.2$ and other values as in Fig. 3. (B) Distribution of activity levels of the cells in the excitatory population in the large K limit for a network of neurons with a bounded distribution of thresholds. The distribution is shown for mean rates $m_E = 0.01$ (solid line) and $m_E = 0.1$ (dashed line). Parameter values as in A. (C) Firing rate distribution for neurons in the right prefrontal cortex of a monkey attending to a complex stimulus (light source and sound) and executing a reaching movement. The rates were averaged over the duration of events that showed a significant response. The average rates was 15.8 Hz.

7.2 Bounded Distribution

We next consider the case of a bounded distribution of thresholds. As an example we take a distribution of θ which is uniform between $-\Delta/2$ and $+\Delta/2$, and zero otherwise. In this case, Eq.(7.8) yields

$$m_k = \frac{1}{\Delta} \int_{-\Delta/2}^{\Delta/2} d\theta \, H\left(\frac{-u_k + \theta}{\sqrt{\alpha_k}}\right) \tag{7.15}$$

To assess the effect of Δ we analyze Eq. (7.15) in the low m_k limit. In this case, the solution for u_k is

$$u_k + \Delta/2 = O(\sqrt{m_k}) \tag{7.16}$$

Thus, the population rates adjust themselves so that synaptic input is slightly below the smallest threshold in the population, $\theta_k - D/2$, see Eq. (3.8). The small gap between the mean synaptic input and the minimal threshold is such that the temporal fluctuations of the network, with the low variance α_k, are sufficient to bring the neurons to threshold levels. Indeed, analyzing the rate distribution for this case we find that it is a unimodal with width $\sqrt{q_k}$ where

$$q_k \propto \Delta \, \alpha_k^{3/2} \tag{7.17}$$

This means that the rate distribution is extremely broad and skewed. The full shape of the rate-distribution is given by

$$\rho_k(m) \approx \frac{\sqrt{\alpha_k/2\Delta^2}}{m\sqrt{|\log m|}} \quad , m_- < m < m_+ \tag{7.18}$$

and zero otherwise. The bounds of m are:

$$m_- \propto \exp(-\Delta^2/(2\alpha_k)) \tag{7.19}$$

$$m_+ \propto \Delta \sqrt{\alpha_k/|\log(\alpha_k)|} \quad >> m_k. \tag{7.20}$$

The above results show that in the case of a bounded threshold distribution, the temporal variability remains strong even in the limit of low mean rates. However, the inhomogeneity does affect strongly the shape of the rate distribution making it more skewed and broad. Figure 11B shows the results of numerical calculation of the rate distribution for the excitatory population, with a uniform distribution of thresholds between $-\Delta/2$ and $\Delta/2$, for different values of mean rates. Comparing Figs. 4, 11A and 11B we see that for moderate mean rates $m_k = 0.1$, Δ does not have a big effect on the shape of the distribution. However, lowering the network mean activity the distribution peak shifts to values which are much smaller then the mean while its tail extends to rates which are of the order of $\sqrt{m_E}$. In contrast, in the case of a homogeneous threshold, lowering the mean rates shifts the peak towards the mean and decreases the width of $\rho(m)$, see Fig. 4. In the case of a Gaussian distribution, lowering the mean rates creates a pronounced bi-modal distribution, characteristic of a frozen state, as seen in Fig. 11A.

In general, for small m_k, a threshold distribution $P(\theta)$ will yield a rate distribution ρ_k for population k, that is given by

$$\rho_k(m) = \sqrt{2\pi} P\left(-\sqrt{\alpha_k}(h(m) + \tilde{h}_k)\right) e^{h^2(m)/2}, \tag{7.21}$$

where $\tilde{h}_k$ is determined by

$$\int dm \, m \rho_k(m) = m_k. \tag{7.22}$$

If $P(\theta)$ has tails that fall off as slow as or slower than than a Gaussian, ρ_k will diverge for $m = 0$ and $m = 1$, while if $P(\theta)$ falls of faster than a Gaussian, ρ_k will be negligible for $m < m_-$ and for $m > m_+$ with, for small m_k, $m_- \ll m_k$ and $m_k \ll m_+ \ll 1$. In this case ρ_k can be approximated by

$$\rho_k(m) \propto \frac{P\left(-\sqrt{\alpha_k}(\sqrt{2\log(m)} - \tilde{h}_k)\right)}{m\sqrt{\log(m)}} \tag{7.23}$$

for $m_- < m < m_+$. Furthermore $P\left(-\sqrt{\alpha_k}(\sqrt{2\log(m)} - \tilde{h}_k)\right)$ varies only slowly with m for these rates.

Thus for a threshold distribution with a tail that falls off faster than a Gaussian the distribution of the rates goes to 0 for $m = 0$ and $m = 1$ and has a long power-law tail that extends up to a rate m_+ that is much larger than the average rate. In contrast if the tails of the distribution fall off as slow as or slower than a Gaussian, the rate distribution will peak at $m = 0$ and $m = 1$ if the average rate is sufficiently low.

7.3 Experimental Rate Distribution

The above results make a clear prediction about the shape of the rate distribution in a local population of neurons that have low mean rates. It seems reasonable to compare these predictions with the distribution of rates in cortical neuronal pools of behaving animals. Figure 11C presents an experimentally determined rate histogram of neurons in the right prefrontal cortex of a monkey (Abeles *et al.* unpublished). The data was taken from periods of time while the monkey was attending to a variety of stimuli (light sources and sound) or was executing simple reaching movements. The average rate (of the neurons that showed any activity during the time of measurement) was 15.8 Hz. The observed histogram has a distinct unimodal skewed shape with a tail extending up to 80 Hz. These results are consistent with the theoretical predictions of Fig. 11B.

8 Chaotic Nature of the Balanced State

The strong temporal fluctuations of the neuronal activity in our model and the resultant fast decay of temporal correlations strongly suggests that the balanced state corresponds to a chaotic attractor. However, to justify characterizing this state as chaotic we need to study the sensitivity of the dynamic trajectory to small perturbations in the initial conditions. If the network evolves to a chaotic attractor small perturbations in the state of the network should grow at least exponentially. Therefore after some time the state of the network is far from the state the network would have been in had it not been perturbed. This definition of chaos is technically speaking inapplicable to a system with discrete degrees of freedom such as ours, since in this case the size of a perturbation of the system state is bounded by the discreteness of the system's state. In our case, the minimum perturbation is changing the state of a single neuron. Nevertheless, in the limit of large network size we can consider such a perturbation as infinitesimal, as described below. We consider two copies of the network. In one copy, the states of the neurons are given by $\sigma^i_{1,k}(t)$; in the other they are given by $\sigma^i_{2,k}(t)$. Both networks have the same connection matrices J^{ij}_{kl} and have the same update schedule. The networks get the same constant input $m_0(t) = m_0$, and are assumed to have reached a balanced state with the same population rates,

$$\frac{1}{N_k}\sum_{i=1}^{N_k} < \sigma_{p,k}^i(t) >= m_k \quad \text{for } p = 1, 2. \tag{8.1}$$

The distance between the network states at time t is defined as

$$\begin{aligned} D_k(t) &= \frac{1}{N_k}\sum_{i=1}^{N_k}\left\langle\left(\sigma_{1,k}^i(t) - \sigma_{2,k}^i(t)\right)^2\right\rangle \\ &= \frac{1}{N_k}\sum_{i=1}^{N_k}\left\{\left\langle\sigma_{1,k}^i(t)\right\rangle + \left\langle\sigma_{2,k}^i(t)\right\rangle - 2\left\langle\sigma_{1,k}^i(t)\sigma_{2,k}^i(t)\right\rangle\right\} \end{aligned} \tag{8.2}$$

Here the angular brackets do *not* mean average over time but average over all initial conditions of the two networks subject to the constraints that each individual network is at equilibrium (*e.g.*, its m_k and q_k have the equilibrium values), and that the distance between the initial states of the two networks equals a given $D_k(0)$. If the network is in a chaotic state, the distance $D_k(t)$ of the cells in population k, defined by Eq. (8.2) should grow at least exponentially for small D_k, The maximum Liapunov exponent λ_L, defined by

$$\lambda_L \equiv \lim_{D_k \to 0} D_k^{-1}\frac{dD_k}{dt}, \tag{8.3}$$

should be positive. Note that in calculating λ_L we will first take the large N limit of D_k and then $D_k \to 0$ limit. To write the dynamics of D_k it is useful to write $D_k(t)$ as

$$D_k(t) = 2(m_k - Q_k(t)) \tag{8.4}$$

where $Q_k(t)$ denotes the *overlap* of the two trajectories. In Appendix A we show that $Q_k(t)$ satisfies an equation similar to that of $q_k(\tau)$, namely,

$$\begin{aligned} \tau_k\frac{dQ_k}{dt} &= -Q_k \\ &+ \int Dx\left[H\left(\frac{-u_k + \sqrt{\gamma_k(t)}x}{\sqrt{\alpha_k - \gamma_k(t)}}\right)\right]^2. \end{aligned} \tag{8.5}$$

with u_k and α_k are as above, and $\gamma_k(t)$ given by

$$\gamma_k(t) = \sum_{l=1}^{2}(J_{kl})^2 Q_l(t) = Q_E(t) + J_k^2 Q_I(t). \tag{8.6}$$

It is easy to see that this equation has two stationary solutions. One is

$$Q_k = m_k \tag{8.7}$$

which corresponds to a fully locked trajectories. This solution is unstable, as will be shown below. The stable fixed-point is

$$Q_k = q_k \tag{8.8}$$

which corresponds to a fully desynchronized trajectories so that at long times the correlations between the two trajectories at the same time are the just those induced by the time-independent average activities. Starting from any nonidentical states, the two trajectories will eventually desynchronize them completely. To find the initial rate of divergence, we expand Eq. (8.5) for small D_k, and find that to leading order, the distances satisfy

$$\tau_k \frac{dD_k}{dt} = \frac{2}{\pi} \frac{e^{-u_k^2/2\alpha_k}}{\sqrt{\alpha_k}} \sqrt{\alpha_k - \gamma_k}\ . \tag{8.9}$$

Since $\alpha_k - \gamma_k \propto D_k$, Eq. (8.9) has a growing solution even if $D_k(0) = 0$. This implies that the Liapunov exponent λ_L is infinitely large in the balanced state. Figure 12 shows the evolution of D_E. As can be seen D_E increases rapidly to the equilibrium value $D_E = 2(m_E - q_E)$, for arbitrarily small initial positive value. This should be contrasted with systems with finite positive Liapunov exponents where the initial rate of growth depends on the magnitude of the initial perturbation of the initial conditions. The divergence of λ_L in our system is related to the discreteness of the degrees of freedom, which implies an infinitely high microscopic gain: a small change in the inputs to a cell can cause a finite change in its state.

9 Tracking of Time Dependent Input

We have shown that for a large range of parameters, a network with synaptic strengths of order $1/\sqrt{K}$ will evolve to a balanced state and investigated some of the characteristics of this state. But so far we have not addressed the question of what the functional advantages of this state might be. Why should a network generate an excitatory input that is much larger than the threshold input and then counterbalances this with a nearly equally large

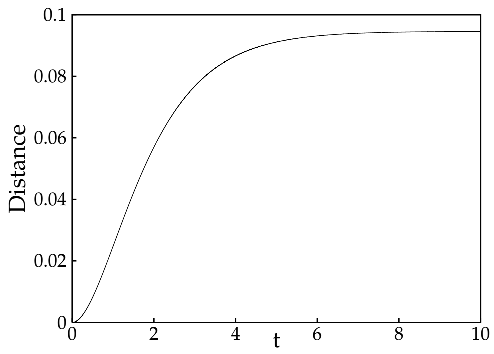

Figure 12: Evolution of the distance D_E starting from a small initial distance in the large K limit. Parameters as in Fig. 3 and $\tau = 0.9$.

inhibitory input? If we consider the metabolic costs of such large currents, it seems clear that a biological system would not choose such a mechanism unless it has some advantages over other mechanisms.

In this section we present one possible advantage of the balanced network. We have already shown that perturbations in the network rates, which are small compared to $1/\sqrt{K}$, die out in a time that is of the order of $1/\sqrt{K}$. Therefore the network is very stable against small fluctuations in the rates. We now consider the consequences of this for the response of the system to time-dependent change in the external driving force m_0.

If the external activity m_0 changes suddenly by a small amount, of the order of $1/\sqrt{K}$, the equilibrium rates will change by an amount that is of the same order. So just after the change in external rate, the network rates differ slightly from the equilibrium rate. They will approach the new equilibrium rate on a time scale that is of the order $1/\sqrt{K}$, so the network rates adapt very fast to a sudden change in m_0. This means that if m_0 changes continuously with time, the network rates will track m_0 very fast, provided that m_0 doesn't change too rapidly. To quantify the speed of the tracking of a balanced network, we compare the network rates with the rates of a hypothetical network that tracks changes in the external rates instantaneously. In such a network the rates m_k^∞ satisfy $m_k^\infty(t) = m_k(m_0(t))$, where $m_k(m_0)$ is the equilibrium rate for $m_0(t) = m_0$ which are given by

$$m_k^\infty(t) = H\left(-\frac{u_k^\infty(t)}{\sqrt{\alpha_k^\infty(t)}}\right), \tag{9.1}$$

with

$$u_k^\infty(t) = \sqrt{K}(J_{k0}m_0(t) + \sum_{l=1}^{2} J_{kl}m_l^\infty(t)) - \theta_k \tag{9.2}$$

and

$$\alpha_k^\infty(t) = \sum_{l=1,2}(J_{kl})^2 m_l^\infty(t). \tag{9.3}$$

Note that to leading order in K m_k^∞ satisfies the balance condition

$$m_k^\infty(t) = A_k\, m_0(t) \tag{9.4}$$

However, Eqs. (9.1)-(9.3) take into account also the $1/\sqrt{K}$ corrections in $m_k^\infty(t)$.

We now assume that

$$m_k(t) = m_k^\infty(t) + m_k^1(t)/\sqrt{K} \tag{9.5}$$

namely, that the deviation from perfect tracking of the instantaneous is only of order $1/\sqrt{K}$. The rates m_k satisfy Eq. (3.3). To leading order in K this is

$$\tau_k\frac{dm_k^\infty(t)}{dt} = -m_k^\infty(t) + H\left(-\frac{u_k^\infty(t) + \sum_l J_{kl}m_l^1(t)}{\sqrt{\alpha_k^\infty(t)}}\right) \quad , k = 1,2. \tag{9.6}$$

Using Eq. (9.4) we obtain

$$A_k\left(\tau_k\frac{dm_0(t)}{dt} + m_0(t)\right) = H\left(-\frac{u_k^\infty(t) + \sum_l J_{kl}m_l^1(t)}{\sqrt{\alpha_k^\infty(t)}}\right) \quad , k = 1,2. \tag{9.7}$$

which determines the small deviations $m_k(t)/\sqrt{K}$ as functions of the time-dependent drive $m_0(t)$. Since $H(x)$ is between 0 and 1 the above equations have a solution only for $0 < m_0 + \tau_k\frac{dm_0}{dt} < 1/A_k$. This implies that the almost

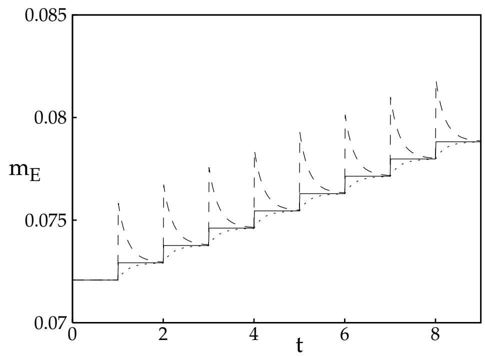

Figure 13: Reaction of the excitatory population to input that is increased by small steps. The solid line shows the activity of a network that responds instantaneously. The dashed line shows the probability P_E of updating to the active state for neurons that happen to update. The dotted line represents the population averaged activity of the population in a balanced network. Parameter values: $K = 1000$, $\tau = 0.9$. Other parameters as in Fig. 3.

perfect tracking occurs for rates of change of the external input which obeys the following bounds

$$\max_{k=1,2} -\frac{m_0}{\tau_k} < \frac{dm_0}{dt} < \min_{k=1,2} \frac{1}{\tau_k} \left(\frac{1}{A_k} - m_0 \right) . \tag{9.8}$$

To understand qualitatively these results, let us consider a system in the balanced state with a fixed m_0 where at time $t = t_0$ m_0 is suddenly changed to $m_0 + \delta m_0$. We assume that δm_0 is much smaller than m_0 but $\delta m_0 \sqrt{K}$ is of order 1. This is shown in Fig. 13 where m_0 is increased by a series of small steps. Because the input is $\sqrt{K} m_0(t)$ the small change in m_0 initially causes a change of order 1 in the total input. Hence the probability P_k that the cells in the k-th population, which are updated at time t_0 will go to the active state is initially increased by a large amount. This is denoted as ΔP_k, namely, ΔP_k is of order 1, as shown by the dashed curve in the figure. In fact, this probability is given by the RHS of Eq. (9.4) which differs substantially from the previous equilibrium probability, $A_k m_0$. This initial increase in the number of active cells is causing a large inhibitory feedback, which causes P_k to decrease fast to its new equilibrium value which only slightly increases from its original equilibrium value, as seen in the figure. Thus, the initial response is highly nonlinear due to the initial disruption of the balance in the inputs and the highly nonlinear dynamics of single cells. This initial large response causes a fast rate of increase in the population rates, since $\delta m_k \approx \tau_k^{-1} dt \Delta P_k$, implying that δm_k reaches the value $A_k \delta m_0$ in time of order $\tau_k/\delta m_0 \approx \tau_k/\sqrt{K}$, see the dotted line in the Figure. The final change in the population rates follows linearly the change in the external input as required to maintain the balance between excitation and inhibition.

The limitation on the change in the external rate is readily explained by the maximum increase (decrease) in the network rate that the microscopic dynamics allows. The fastest the network rates can increase (decrease), is by putting all newly updated cells in the active (passive) state, *i.e.,* $P_k = 1$ ($P_k = 0$), so that the change in the network rates is bounded by

$$-m_k < \tau_k \frac{dm_k}{dt} < 1 - m_k. \tag{9.9}$$

If the external rates increase (decrease) faster than the bound Eqs. (9.8) the network will not stay in the balanced state during the rate change, so that u_k is of order $\sqrt{K}$. Consequently, the input is above (below) the threshold for all cells of the kth population that are updated, and all updated cells are in the active (passive) state.

To compare the tracking capabilities of balanced networks with those of an unbalanced network, we consider a network of threshold linear neurons with synapses of strength J_{kl}/K for inter-network connections and $\tilde{J}_{k0}/K$ for the strengths of the synapses projecting from the external population and the thresholds T_k chosen so that the equilibrium rates of this network is the same as those for the balanced network. We choose the same neuronal time constants as in the balanced network. In this network the rates satisfy

$$\tau_k \frac{dm_k}{dt} = -m_k + (\tilde{J}_{k0} m_0 - J_{kE} m_E + J_{kI} m_I + T_k)_+, \tag{9.10}$$

with $(x)_+ = (x + |x|)/2$. If we set $m_k(t) = m_k^\infty(m_0(t)) + m_k^1(t)$, the difference between the network rates and the rates of a perfectly tracking network, $m_k^1(t)$, satisfy

$$\tau_E \frac{dm_E^1}{dt} = (J_{EE} - 1) m_E^1 + J_{EI} m_I^1 - \tau_E A_E \frac{dm_0}{dt} \tag{9.11}$$

$$\tau_I \frac{dm_I^1}{dt} = J_{IE} m_E^1 + (J_{II} - 1) m_I^1 - \tau_I A_I \frac{dm_0}{dt}. \tag{9.12}$$

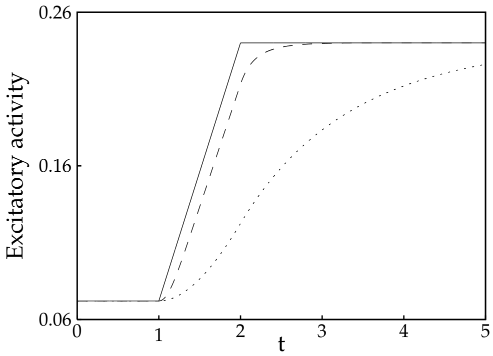

Figure 14: Population averaged activity of the excitatory cells for an input that varies with time The input is constant from time $t = 0$ to $t = 1$. Between $t = 1$ and $t = 2$ the input increases linearly. After $t = 2$ the input is again constant. The solid line shows the excitatory rate of a network that responds infinitely quickly, the dashed line shows the response of the balanced network. Also shown is the response of an unbalanced network of threshold linear neurons (dotted line). Parameters for the balanced network as in Fig. 13. For the unbalanced network see text.

e.i. m_k^1 will be of order 1.

Thus in the unbalanced network the difference between the network rates and the rates in a perfectly tracking network will be of order $\sqrt{K}$ times larger than in a balanced network.

Figures 14 and 15 show a comparison of the tracking capabilities of a balanced network with $K = 1000$ and an unbalanced network with threshold linear units. Between $t = 0$ and $t = 1$ the networks are at equilibrium. In Fig. 14 the external activity is ramped between $t = 1$ and $t = 2$,

$$m_0(t) = m_0 + v_0 t \tag{9.13}$$

and after $t = 2$ m_0 is kept constant again. The graph shows m_E^∞ and m_E for both networks plotted against time. Clearly the balanced network is much better in tracking the change in external rate than the unbalanced network. Similar results are seen in the case of a sinusoidal external input, Fig. 15. Finally, in Fig. 16 we plot the rate of change of m_E vs. v_0 for the ramped input case. The results of this as well as Figs. 14 and 15 are based on a full finite K solution of the dynamics. We also show in Fig. 16 the large K predictions according to which there is a sharp upper bound for fast tracking at a value of v_0 given in Eq. (9.8).

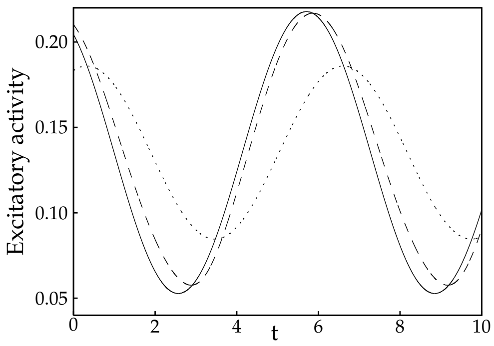

Figure 15: Average rate of the excitatory population for a sinusoidally varying input. The rates of the excitatory population in an instantaneously responding network (solid line), a balanced network (dashed line), and an unbalanced network (dotted line) are shown. Parameters as in Fig. 15

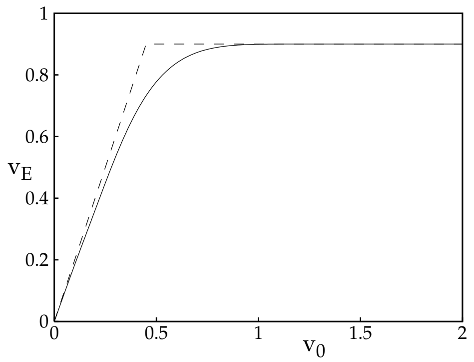

Figure 16: Rate v_E with which the average excitatory rate changes as a function of the rate of change v_0 of the external input. The solid line shows v_E for a network with $K = 1000$, the dashed line shows the same for the large K limit. Parameters as in Fig. 15.

10 Discussion

10.1 Asynchronous and Synchronized Chaos

The purpose of our theory is to identify the different mechanisms by which the deterministic dynamics generates strongly irregular states in large neural networks, in which each cell receives input from many other cells. To understand these mechanisms from a theoretical point of view it is important to study the network behavior in the limits of large system size N and large connectivity index K. In a finite network with fluctuating dynamics there will always be some degree of synchrony and some compensation between inhibition and excitation. It is thus impossible to single out balancing between excitation and inhibition as a mechanism for variability which is separate from synchronized chaos (Bush and Douglas 1991, Hansel and Sompolinsky 1992,1996). It is only in the limit of large N, where states with synchrony that does not vanish in this limit can be distinguished from states where the synchrony does vanish, that the different mechanisms become clearly separate. Likewise, the importance of the limit of large K is that for fixed finite K, network parameters may be tuned so that fluctuations in individual synaptic inputs generate fluctuations in the membrane potential of the post-synaptic cells. These fluctuations can be due to stochastic synaptic failures or variability in the presynaptic cells from within or outside the network. In other words, for a finite fixed K the issue of balancing between excitation and inhibition is a quantitative issue. Only in the large K limit is there a clear separation in the balanced state between the distance between the net input from threshold and the corresponding distance of each of the excitatory and inhibitory components.

The outcome of the present theory combined with our previous studies is that chaotic states in large highly connected networks can be classified as *synchronized chaos* and *asynchronous chaos*. Synchronized chaos is likely to occur in fully connected networks, where K is proportional to N, yielding a strong overlap between inputs to different neurons. In this case, the chaotic state is characterized by cross-correlations between neuronal pairs whose amplitude is of order 1 even in the limit of $N \to \infty$, thereby creating strong fluctuations of the common feedback. Thus, synchronized chaos can be viewed as resulting from an instability in the dynamics of the macroscopic degrees of freedom that comprises the common fluctuating mean-field.

Asynchronous chaotic states are distinguished by the weak cross-correlations. In the present case this is due to the sparseness of the connections. More specifically, in our networks the amplitude of the cross-correlations has a broad distribution in the network due to inhomogeneity in the connectivity. Most of the cross-correlations are of the order $1/N$ where N is the network size. The maximal value of the cross-correlations occurs for pairs that are directly connected and this cross-correlation is of the order of the strength of the synapse, *i.e.,* $O(1/\sqrt{K})$. Thus, chaos in this state is the result of instability in local degrees of freedom, similar to chaos in asymmetric spin-glasses and neural networks.

10.2 Balanced State with Strong or Weak Synapses

The scaling of connection strength in our theory of the balanced state is different from conventional mean-field theories of highly connected networks. Most mean-field theories of large, highly connected neural networks assume that each connection is scaled as the inverse of the mean number of inputs to a neuron, K. In contrast, we scale the connections as $1/\sqrt{K}$. This aspect, together with the relative sparseness of the connections, and the asynchrony of the dynamics yields a highly irregular dynamical state, despite the fact that the single neuron dynamics in our model is the simple threshold updates of binary units. The presence of relatively large connections is again analogous to the scaling of connections in highly connected spin-glasses and random neural networks, where the interactions have to scale as the inverse square root of the connectivity index (Derrida *et al.* 1987, Sompolinsky *et al.* 1988). In Sompolinsky *et al.* (1988) the network is a fully connected asymmetric analog circuit with connections that are independent random variables with zero mean. The connections posses a square-root scaling with the number of inputs, as is natural for mean-field spin-glasses (Mezard *et al.* 1987). In Derrida *et al.* (1987) the connectivity is randomly sparse as is in our model. The connections store random memories so that in the limit of a large K (and correspondingly large number of stored patterns) they are effectively random in sign, and exhibit chaotic dynamics similar to the asymmetric spin-glass. In contrast, in our case the connections are not random in sign but are organized in an excitatory- inhibitory two-population architecture. Consequently, the balance between excitation and inhibition which gives rise to the temporally disordered state is entirely a dynamic effect. Our results should be contrasted

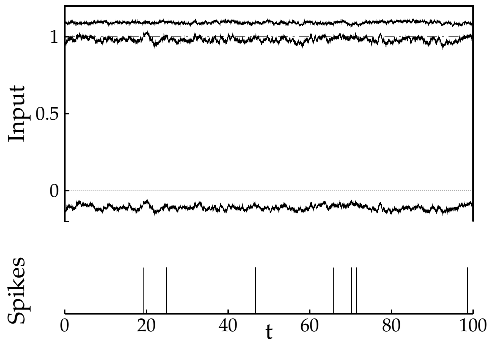

Figure 17: Inputs to an excitatory cell in a network with synaptic strengths J_{kl}/K. The total excitatory inpit (upper trace), the total inhibitory input (lower trace) and the net input (middle trace) are shown in the upper panel. At the bottom, the times when the cell switches from the passive to the active states are indicated. Parameters: $K = 1000$, $E = 2.0$, $I = 1.6$, $J_E = 2.0$, $J_I = 1,8$, $\theta_E = 1.0$, $\theta_I = 0.8$, $\tau = 0.9$, and $m_0 = 0.503$.

with a conventional, fully connected network with with the same simple two-population architecture with more conventional $1/K$ scaling of connections. Such networks converges to either static states or globally coherent limit cycles. (Abbott and Van Vreeswijk 1993, Gerstner and Van Hemmen 1993, Grannan *et al.* 1992, Hansel *et al.* 1995, Van Vreeswijk 1996, Wilson and Cowan 1972).

An important consequence of our assumption of relatively strong synaptic connections is concerned with the size of the external input to the local network. According to our theory, the balanced state is robust only when the DC external input to the local network is large, *i.e.,* of the same order as the local excitatory and inhibitory feedback, and much larger than the *net* synaptic input to a cell. In the notation of our model, the external input to an excitatory cell is $Em_0\sqrt{K}$ whereas the net input to this cell, u_E is smaller than the external input by a factor of the order of $1/(m_0\sqrt{K})$, where m_0 is the rate of an input cell and is assumed to be much larger than $1/\sqrt{K}$. Figure 3 shows that lowering the strength of the external input *i.e.,* reducing m_0, will turn off the activity of the network. In fact, Eq. (3.3) implies that to maintain the balanced activity in the case of an external input which is only of order 1 requires the vanishing of the denominators in Eqs. (4.3) and (4.4) which means that the interaction strengths have to be fine tuned to a very narrow range.

Because of the importance of the scaling of the synapses in our theory, it is very informative to consider the behavior of our model if we use a conventional scaling of synapses *i.e,* that each synapse scales as $1/K$, the *weak synapses* scenario. In this scenario, each component of the synaptic inputs, including the total external input to a cell is of order 1. The solution of this model (Van Vreeswijk and Sompolinsky unpublished) shows that when K is not large, the network settles in a strongly disordered state. This is not surprising given that the connectivity is randomly asymmetric and there is no danger of averaging of the fluctuating inputs to a cell. However, the fate of the temporal variability as K is increased is highly sensitive to the presence of local inhomogeneity. *If the neurons have the same threshold*, the chaotic state is maintained as K increases. In this case, the population rates adjust their value so that the net input is close to the threshold level within a distance of the order of $1/\sqrt{K}$. This is shown in Fig. 17. This figure displays the time course of the various synaptic inputs to a cell, evaluated by simulating a sample from the statistics predicted by the mean-field solution with the weak-synapses scaling. The results of this figure should be contrasted with the behavior of the strong synapses scenario, Fig. 6. In Fig. 17 the variability is caused by the fact that the cell is always hovering close to its threshold. In contrast, in the case of Fig. 6 the distance between the net input and the threshold is not small compared to the distance between threshold and rest. In this case, the variability is caused by the presence of excitatory and inhibitory inputs each of which is much larger than the threshold.

Despite the difference in behavior between the two scenarios, the dynamic mechanism for these balanced chaotic states is the same. In both cases, the distance between the net input and the threshold is smaller (by a factor of $1/\sqrt{K}$) from the distance to threshold of the excitatory and inhibitory components. Thus, it would seem that choosing between these scenarios is largely a matter of biological interpretation. However, there are some qualitative difference between the two scenarios. Since the synaptic inputs are all of the same order as the threshold, it is harder to obtain states with low mean rates in both the excitatory and inhibitory populations. To achieve low rates, the ratio between the external inputs to the two populations (I/E in the notation of Eqs. (2.4)) and (2.5) has to be close to the ratio of their thresholds θ_I/θ_E. More importantly, the weak-synapses scenario of Fig. 17 breaks down in the presence of inhomogeneity in the local thresholds. In this case the population rates are incapable of accommodating the different thresholds. As a result, in the case of inhomogeneous thresholds, when K increases the network state becomes increasingly frozen; neurons with high thresholds become inactive whereas neurons with low ones fire close to saturation. This freezing occurs as soon as the width of the inhomogeneity in threshold is larger than $1/\sqrt{K}$. In contrast, in the scenario of strong synapses we assume, the state only becomes frozen when the inhomogeneity is large compared to 1. Note that in the case of Fig. 17 the external input is of the same order as the net input to the cell. Equally important is the fact that in the weak scenario case and homogeneous networks, the collective time constants are of order of the single cell time constant so that the network will not exhibit the phenomenon of fast tracking predicted in our theory.

Finally the model can be generalized to a model with synaptic strengths that scale as $K^{-\alpha}$, with $0 < \alpha < 1$. Of course these models can only be distinguished from the present model in the large K limit. In this limit the net average inputs into the populations scale as $K^{1-\alpha}$, while the quenched and temporal fluctuation in the inputs scale as $K^{1/2-\alpha}$. Therefore the leading order in the inputs have to cancel, leading to the balance condition. For any α this leads to asynchronous chaotic activity in a homogeneous network, similar to the case $\alpha = 1/2$. However if we introduce a distribution of the threshold with width of order 1, we have to distinguish two regimes, apart from $\alpha = 1/2$ of our model. If $\alpha > 1/2$ the fluctuations in the input decrease with K so that the network goes to the frozen state in the large K limit. On the other hand, if $\alpha < 1/2$ the fluctuations grow with K, and therefore the inhomogeneity in the threshold becomes negligible in the large K limit. Thus a network with inhomogeneous threshold will act the same way as a network with homogeneous thresholds. Specifically for low rates the rate distribution will become narrow. Thus only for a network with synaptic strengths of order $1/\sqrt{K}$ is there a nontrivial interaction between the fluctuation in the input and the threshold inhomogeneities.

10.3 Comparison with Other Network Models

Some of our results are consistent with those of the Integrate-and-Fire network models of Tsodyks and Sejnowski (1995) and Amit and Brunel (1996a,b). Although constructing an exact mean-field theory for the Integrate-and-Fire dynamics similar to the one presented here for binary units is much more difficult, we believe that most of the predictions of our mean-field theory are applicable to the Integrate-and-Fire dynamics as well, provided the the same connectivity architecture and scaling of parameters with N and K are used. However, a direct comparison between our theory and the results of Tsodyks and Sejnowski (1995) and Amit and Brunel (1996a,b) is difficult, because of their introduction of stochasticity in the network, the combination of mechanisms such as resetting potential close to threshold, and the lack of full explicit specification of scaling of parameters with N and K. Tsodyks and Sejnowski show numerically that their model is capable of 'fast switching' in response to a fast change in the external stimulus. This may be related to the fast tracking predicted in our model. The fact that our model does not respond fast to a sudden switching of the stimulus (see Fig. 13) is probably a result of the dynamics of binary neurons. However, the switching time constants observed in Tsodyks and Sejnowski (1995) is of the same order as the single cell integration time constant, while the fast tracking should occur on a much shorter time constant. In recent numerical simulations of Integrate-and-Fire Networks Amit and Brunel (1996b) show that the strength of the average cross-correlations decreases as N increases, (keeping the connectivity index constant). However, they do not show whether as N increases, the variability in the single cell remains the same. If this would be the case then, their results are consistent with our predictions regarding asynchronous chaotic state.

10.4 Biological Implications

With regards to the biological systems we should reemphasize that most likely temporal irregularity is a result of several mechanisms including those mentioned in the Introduction. Our discussion above makes it clear that even with regards to deterministic network mechanism in a finite system the temporally irregular state is likely to be at best intermediate between the synchronized and the balanced chaotic states. As discussed above, an important question is whether external input is large relative to net input to a cortical cell. Recent experimental findings of Ferster *et al.* (1996) in cat primary visual cortex suggest that the input from LGN to Layer 4 cortical cells are in fact a fraction of the net input. Stratford *er al.* (1996) show that the total strength of the LGN synapses is about 2.5 to 3 times smaller than the total strength of the excitatory feedback synapses from layer 4 cells, however this study does not measure the strength of the feedback from the inhibitory interneurons so it does not allow for the estimation of the net feedback. Further experimental clarification of this issue is called for. Measurements of the distribution of time-averaged rates within a local population of neurons and the change in its shape when the over-all level of response increases, similar to those of Fig. 11B, would be an interesting test of the underlying statistical characteristics of the network spatio-temporal fluctuations.

10.5 Future Work

On theoretical grounds our work raises several interesting issues that are worth pursuing. First, it would be important to know whether the theory of the balanced state applies also to networks with more interesting connectivity architecture. Thus, it would be interesting to extend our theory to networks that model associative memory or hypercolumns in visual cortex. It is important to study the consequences of nonlinearities of synaptic summations, *e.g.,* by treating synaptic inputs as conductance changes instead of currents.

In considering the functional implications of our theory it is important to distinguish between the sensitivity of a chaotic autonomous system to changes in its initial condition and its ability to lock to a changing external drive. The analysis of tracking capabilities of our network shows that the macroscopic state of the network responds fast to a changing input. In the case of a homogeneous input it can be shown that the microscopic state is not tightly locked to the changing stimulus. On the other hand, preliminary analysis (Van Vreeswijk and Sompolinsky unpublished) shows that in the case of spatially inhomogeneous input fluctuations the microscopic state of the network will tightly lock to the stimulus temporal variations. These findings are consistent with recent findings that cortical cells respond highly reliably to the fluctuations in the stimulus (Bair and Koch 1996, Britten *et al.* 1994). Elucidation of the computational aspects of balanced states in neuronal networks is a challenging issue.

Recently Markram and Tsodyks (1996) have shown that the synapses between cortical pyramidal cells show a marked degree of depression. It should be investigated how such dynamical synapses affect the balanced state. If one assumes synaptic depression between the excitatory-to-excitatory synapses only, and facilitation between the synapses from the inhibitory to the excitatory and from the excitatory to inhibitory populations (Thomson *et al.* 1995,1996), the equilibrium rates in the network decrease, relative to those in a network without facilitation. This synaptic depression and facilitation also has the effect that the constraints on the synaptic strengths Eqs. (4.9) and (4.10) can be relaxed. Because the synaptic depression and facilitation only become effective on a time scale that is as slow as or slower than the membrane time constant, the response of such a network to an external input that changes with time is more complicated that in the model studied here. If the input is suddenly increased by a small amount, the network rates increase to the rate the network would have in equilibrium if the synaptic strenghts were not changed in a time of order $1/\sqrt{K}$ and then, on a much slower time scale the rates decrease due to the change in the synaptic strengths.

It should be noted that, since in the balanced state the finite K corrections of the rates are determined by both the first and the second moment of input, the change in rate due to synaptic depression/facilitation depends not only the average change in the synaptic strength, but also its fluctuation. Thus synaptic depression due to a change in the height of the EPSPs, but without a change in the probability of release will affect the rates differently from synaptic depression that leaves the height of the EPSPs unaffected but decreases the probability of release, even if both mechanisms result in the same average depression. An other effect of synaptic depression that will have to be taken into account, is that it will decrease the fluctuations in the input, since the effect of of the second spike in decreased if it follows shortly after the first spike. This will give rise to negative correlations in the input, even if the presynaptic cells fire Poissonian. This leads to decreased fluctuations. Facilitation, on the other hand, will enhance the fluctuations. These issues warrant further study.

Acknowledgments

We thank D.J. Amit, D. Hansel and T. Sejnowski, and M. Tsodyks for very helpful discussions. We are grateful to M. Abeles, H. Bergman and E. Vaadia for permission to present their data. This work is partially supported by the Fund for Basic Research of the Israeli Academy of Science.

Appendix A: Derivation of the Mean-Field Theory

A.1 Population Rates

We first consider the population-averaged activities $m_E(t)$ and $m_I(t)$ in the limit of large N_E and N_I and finite K. We first assume that each cell in the k-th population is updated stochastically at a rate τ_k. When a cell is updated it moves to the active state if its total input is above threshold. Otherwise, its updated state is 0. It is convenient to define a time-dependent local rate variable,

$$m_k^i(t) =< \sigma_k^i(t) > \tag{A.1}$$

Here, the symbol $< ... >$ does not mean average over time, as in Eq. (5.4) and thereafter. Instead, here it means average over all initial conditions that are consistent with given values for $m_k(0)$ and also over the random sequence of update times. It is well known that the rate of a binary variable which obeys the above update rule satisfies the following continuous time dynamics (Ginzburg and Sompolinsky 1994, Glauber 1963)

$$\tau_k \frac{d}{dt} m_k^i(t) = -m_k^i(t) + \Theta(u_k^i(t)) \tag{A.2}$$

where $u_k^i(t)$ is the total synaptic input into a cell i in the k-th population relative to its threshold, and is given in our case by Eq. (2.2). If a cell receives $n_E(t)$ and $n_I(t)$ excitatory and inhibitory feedback inputs, respectively, then its input is

$$u_k^i(t) = \sqrt{K} J_{k0} m_0 + \frac{J_{kE}}{\sqrt{K}} n_E(t) + \frac{J_{kI}}{\sqrt{K}} n_I(t) - \theta_k \tag{A.3}$$

The main assumption underlying the mean-field theory is that the activities of the different input cells to a given cell are uncorrelated. Technically, this holds rigorously provided that $K \ll \log N_k$ (Derrida *et al.* 1987). Using this assumption, the population average of Eq. (A.2) yields the following mean-field equations for the population activities

$$\tau_k \frac{d}{dt} m_k(t) = -m_k(t) + F_k(m_E(t), m_I(t)). \tag{A.4}$$

where F_k denotes the probability that the updating cell at time t will be in an updated active state. It is given by

$$F_k(m_E, m_I) = \sum_{n_1, n_2 = 0}^{\infty} p_1(n_1) p_2(n_2) \Theta\left(\sqrt{K} J_{k0} m_0 + \sum_l \frac{J_{kl}}{\sqrt{K}} n_l - \theta_k\right) \tag{A.5}$$

where $p_l(n)$ is the probability that a cell receives n active inputs from the l-th population.

For $N_E, N_I \to \infty$ the probability of s synapses of population l projecting to a cell is $K^s e^{-K}/s!$. On average each of these synapses has a probability m_l to be active, hence

$$\begin{aligned} p_l(n) &= \sum_{s=n}^{\infty} \frac{K^s}{s!} e^{-K} \begin{pmatrix} s \\ n \end{pmatrix} m_l^n (1-m_l)^{s-n} \\ &= \frac{(m_l K)^n}{n!} e^{-m_l K}. \end{aligned} \tag{A.6}$$

Equations (A.4)-(A.6) define the mean-field equations for the population activity levels for finite K. The average values of n_E and n_I satisfy $< n_k >= m_k K$. The standard deviations $\sigma(n_E)$ and $\sigma(n_I)$ are given by $\sigma(n_k) = m_k K$. In the large K limit the probability distributions $p_k(n)$ can be replaced by Gaussian distributions. According to Eq. (A.6), the means and variances of this distribution are $[n_k] = [(\delta n_k)^2] = K m_k$. Therefore, in the limit $K \to \infty$, $F_k(m_E, m_I)$ is given by

$$F_k(m_E, m_I) = \int Dx\, \Theta(u_k + \sqrt{\alpha_k} x) \;=\; H\left(\frac{-u_k}{\sqrt{\alpha_k}}\right). \tag{A.7}$$

where $Dx = dx \exp(-x^2/2)/\sqrt{2\pi}$. From the above statistics of n_l, one obtains that the average input, relative to threshold, u_k into a cell of population k given by

$$u_k = (J_{k0} m_0 + J_{kE} m_E + J_{kI} m_I)\sqrt{K} - \theta_k \tag{A.8}$$

and standard deviation of the input α_k

$$\alpha_k = (J_{kE})^2 m_E + (J_{kI})^2 m_I. \tag{A.9}$$

from which Eqs. (3.3)-(3.6) follow.

A.2 Auto-Correlations

We now extend the above analysis to evaluate the dynamics of the auto-correlation function $q_k(\tau)$, Eqs. (5.16). Using similar arguments as for Eq. (A.2), $q_k(\tau)$ satisfies an equation of the following form

$$\tau_k \frac{dq_k}{d\tau} = -q_k(\tau) + \int_0^{\infty} \frac{dt'}{\tau_k} \exp(-t'/\tau_k)\, F_k(\{m_l\}; \{q_l(t' + \tau)\}). \tag{A.10}$$

where

$$F_k = \left[\left\langle \Theta(u_k^i(t))\Theta(u_k^i(t+t'+\tau)) \right\rangle \right] \tag{A.11}$$

Here the averaging is also over absolute time t. The integral over time in the RHS of the above equation takes into account the correlation between the inputs to a cell that updates its state at time $t+\tau$ and its inputs at the *last update before time* t. Thus, the time integral is an integral over the exponential distribution of update interval of the last update before time t. Separating the total number of active inputs into those that come from sources in the k-th population that are active in both times ($n_{1,k}$) and those that are active only in one of the times ($n_{2,k}$ and $n_{3,k}$, respectively), one can write

$$\begin{aligned} F_k &= \prod_{l=1,2} \sum_{n_{kl}} p_l(n_{1l}, n_{2l}, n_{3l}) \Theta\left(\sqrt{K} J_{k0} m_0 + \sum_l \frac{J_{kl}}{\sqrt{K}} (n_{1l} + n_{2l}) - \theta_k\right) \times \\ & \Theta\left(\sqrt{K} J_{k0} m_0 + \sum_l \frac{J_{kl}}{\sqrt{K}} (n_{1l} + n_{3l}) - \theta_k\right). \end{aligned} \tag{A.12}$$

where

$$p_l(n_1, n_2, n_3) = \frac{(q_l K)^{n_1}}{n_1!} \frac{((m_l - q_l)K)^{n_2+n_3}}{n_2! n_3!} e^{-(2m_l - q_l)K}. \tag{A.13}$$

In the large K limit this can be written as

$$\begin{aligned} F_k &= \int Dx_1 \int Dx_2 \int Dx_3 \Theta(u_k + \sqrt{\beta_k} x_1 + \sqrt{\alpha_k - \beta_k} x_2 - \theta_k) \times \\ & \Theta(u_k + \sqrt{\beta_k} x_1 + \sqrt{\alpha_k - \beta_k} x_3 - \theta_k) \\ &= \int Dx \left[H\left(\frac{\theta_k - u_k - \sqrt{\beta_k} x}{\sqrt{\alpha_k - \beta_k}}\right)\right]^2, \end{aligned} \tag{A.14}$$

with u_k and α_k as above, and β_k given by

$$\beta_k(\tau) = \sum_{l=1,2} (J_{kl})^2 q_l(\tau). \tag{A.15}$$

So that q_k satisfies Eq. (5.17).

A.3 Sensitivity to Initial Conditions

The derivation of Eq. (8.5) for the overlaps $Q_k(t) = (m_k + D_k)/2$ of two trajectories Eq. (8.2) which start with slightly different initial conditions, is similar to that of q_k. Here the inputs $n_{1,k}$ are the sources to a given cell that are active at time t in both trajectories. The only difference between the equation for the delayed-time autocorrelations and the equal-time overlap between two trajectories is the integral over the previous update times which appears in (A.10) and (5.17). This results from the fact that in the latter case the update sequence is identical in the two trajectories.

Appendix B: Determinstic Update Rules

The general form of Eq. (A.4) is usually derived for a binary variable that is updated stochastically at a rate τ_k. One might therefore argue that the irregular firing in our model is due to the stochasticity of the update times of the model neurons. To show that this is not the case we define here a completely *deterministic* dynamic model and show that it leads to exactly the same equations for the mean rates of activity as those given above.

Consider the same network model, except that a neuron i of population k is updated at times $t = (n + \delta_k^i)\tau_k$ with $n = 0, 1, 2, \ldots$ and δ_k^i is randomly chosen between 0 and 1. Let $m_k^+(t)$ be the probability that the neuron of population k, that is updated at time t, goes into (or stays in) the active state. Since all neurons of population k are updated exactly once between times $t - \tau_k$ and t, $m_k(t)$ is given by

$$m_k(t) = \frac{1}{\tau_k} \int_0^{\tau_k} dt' m_k^+(t - t') \tag{B.1}$$

Going through arguments similar to those shown above, one can show that m_k satisfies

$$m_k(t) = \frac{1}{\tau_k} \int_0^{\tau_k} dt' F_k(m_E(t - t'), m_I(t - t')) \tag{B.2}$$

with F_k given by Eqn. (A.5).

If we introduce inhomogeneities in the rate with which the cells are updated so that cell i of population is updated at times $t = (n + \delta_k^i)\tau_i^k$, where

τ_i^k has a probability $R_k(\tau)d\tau$ of being between τ and $\tau + d\tau$ we find that m_k evolves as

$$m_k(t) = \int_0^\infty d\tau \frac{R_k(\tau)}{\tau} \int_0^\tau dt' F_k(m_E(t-t'), m_I(t-t')). \tag{B.3}$$

For $R_k(t) = te^{-t/\tau_k}/\tau_k^2$ this can be written as

$$m_k(t) = \frac{1}{\tau_k} \int_0^\infty dt' e^{-t/\tau_k} F_k(m_E(t-t'), m_I(t-t')), \tag{B.4}$$

and this is equivalent to Eqn. (A.4).

Thus in this completely deterministic model the mean rates m_k satisfy exactly the same equations as the model with stochastic updating. This also holds true for the other mean field equations of the model.

References

[1] Abbott, L.F. and van Vreeswijk, C. 1993. Asynchronous states in networks of pulse-coupled oscillators. *Phys. Rev. E* **48**, 1483-1490.

[2] Abeles, M. 1991. *Corticonics: Neural Circuits of the Cerebral Cortex.* (Cambridge University Press, Cambridge).

[3] Abeles, M., Bergman, H., and Vaadia, E. unpublished data.

[4] Amit, D.J. and Brunel, N. 1996a. Model of global spontaneous activity and local structured activity during delay periods in the cerebral cortex *Cereb. Cortex* **7** 237-252.

[5] Amit, D.J. and Brunel, N. 1996b. Dynamics of a recurrent network of spiking neurons before and following learning. Preprint.

[6] Bair, W., Koch, C., Newsome, W., and Britten, K. 1994. Power spectrum analysis of bursting cells in area MT in the behaving monkey. *J. Neurosci.* **14**, 2870-2892.

[7] Bair, W. and Koch, C. 1996. Temporal precision of spike trains in extrastriate cortex of the behaving Macaque monkey. *Neural Comput.* **8**, 1185-1202.

[8] A. Bell, A., Mainen, Z.F., Tsodyks, M., and Sejnowski, T. 1994. *Soc. Neurosci. Abstr.* **20**, 1527.

[9] Britten, K.H., Shadlen, M.J., Newsome, W.T., and Movshon, J.A. 1992. The analysis of visual motion: A comparison of neuronal and psychophysical performance. *J. Neurosci.* **12**, 4745-4765.

[10] Burns, B.D. and Webb, A.C. 1976. The spontaneous activity of neurons in the cat's visual cortex. *Proc. R. Soc. Lond. B* **194**, 211-223.

[11] Bush, P.C. and Douglas, R.J. 1991. Synchronization of bursting action potential discharge in a model network of neocortical neurons. *Neural Comp.* **3**, 19-30.

[12] Derrida, B., Gardner, E., and Zippelius, A. 1987. An exactly soluble asymmetric neural network model. *Europhys. Lett.* **4** 167-173.

[13] Douglas, R.J. and Martin, K.A.C. 1991. Opening the grey box. *Trends in Neurosci.* **14**, 286-293.

[14] Douglas, R.J., Martin, K.A.C., and Whitteridge, D. 1991. An intracellular analysis of the visual response of neurons in cat visual cortex. *J. Physiol.* **440**, 659-696.

[15] Ermentrout, J.B. and Gutkin, B. 1997. Preprint.

[16] Ferster, D., Chung, S., and Wheat, H. 1996. Orientation selectivity of thalamic input to simple cells of cat visual cortex. *Nature* **380**, 249-252.

[17] Ferster, D. and Jagadeesh, B. 1992. EPSP-IPSP interactions in cat visual cortex studied with *in vivo* whole-cell patch recording. *J. Neurosci.* **12**, 1262-1274.

[18] Gerstein, G.L. and Mandelbrot, B. 1964. Random walk models for the spike activity of a single cell. *Biophys. J.* **4**, 41-68.

[19] Gerstner, W. and van Hemmen, J.L. 1993. Associative memory in a network of 'spiking' neurons. *Network* **3**, 139-164.

[20] Ginzburg, I. and Sompolinsky, H. 1994. Theory of correlations in stochastic neural networks. *Phys. Rev. E* **50**, 3171-3190.

[21] Glauber, R.J. 1963. Time-dependent statistics of the Ising model. *J. Math. Phys.* **4**, 294-307.

[22] Grannan, E., Kleinfeld, D., and Sompolinsky, H. 1992. Stimulus-dependent synchronization of neuronal assemblies. *Neural Comp.* **4**, 550-569.

[23] C.M. Gray and W. Singer, W. 1989. Oscillatory responses in cat visual cortex exhibit inter-columnar synchronization which reflects global stimulus properties. *Nature* **338**.334-337.

[24] Hansel, D., Mato, G., and Meunier, C. 1995. Synchronization in excitatory neural networks. *Neural Comp.* **3**, 307-338.

[25] Hansel, D. and Sompolinsky, H. 1992. Synchronization and computation in a chaotic neural network. *Phys. Rev. Lett.* **68**, 718-721.

[26] Hansel, D. and Sompolinsky, H. 1996. Chaos and synchrony in a model of a hypercolumn in visual cortex. *J. Comput. Neurosci.* **3**, 7-34.

[27] Holt, G.R., Softky, W.R., Koch, C.,and Douglas, R.J. 1996. A comparison of discharge variability *in vitro* and *in vivo* in cat visual cortex neurons. *J. Neurophysiol.* **75**, 1806-1814.

[28] Mainen, Z.J. and T. Sejnowski, T. 1995. Reliability of spike timing in neocortical neurons. *Science* **268**, 1503-1506.

[29] Markram, H. and Tsodyks, M. 1996. Redistribution of synaptic efficacy between neocortical pyramidal neurons. *Nature* **382**, 807-810.

[30] Mézard, M., Parisi, G., and Virasoro, M.A. 1987. *Spin Glass Theory and Beyond.* (World Scientific, Singapore).

[31] Perkel, D.H., Gerstein, G.L., and Moore, G.P. 1967a. Neuronal spike trains and stochastic pointprocesses. I. The single spike train. *Biophys J.* **7**, 391-418.

[32] Perkel, D.H., Gerstein, G.L., and Moore, G.P. 1967b. Neuronal spike trains and stochastic pointprocesses. II. Simultaneous spike trains. *Biophys J.* **7**, 419-440.

[33] Shadlen, M.N. and Newsome, W.T. 1994. Noise, neural codes and cortical organization. *Curr. Opin. Neurobiol.* **4**, 569-579.

[34] Shadlen, M.N. and Newsome, W.T. 1995. Is there a signal in the noise? *Curr. Opin. Neurobiol.* **5**, 248-250.

[35] Softky, W.R. 1995. Simple codes versus efficient codes. *Curr. Opin. Neurobiol.* **5**, 239-247.

[36] Softky, W.R. and Koch, C. 1993. The highly irregular firing of cortical cells is inconsistent with temporal integration of random EPSPs. *J. Neurosc.* **13**, 334-350.

[37] Sompolinsky, H., Crisanti, A., and Sommers, H.J. 1988. Chaos in neural networks *Phys. Rev. Lett.* **61**, 259-262.

[38] Stratfort, K.J., Tarczy-Hornoch, K. Martin, K.A.C., Bannister, N.J., and Jack, J.J.B. 1996. Excitatory synaptic inputs to spiny stellate cells in cat visual cortex *Nature* **382**, 258-261.

[39] Thomson, A.M., West, D.C., and Deuchars, J. 1995. Properties of single axon excitatory postsynaptic potentials elicited in spiny interneurons by action potentials in pyramidal neurons in slices of rat neocortex. *Neurosci.* **69**, 727-738.

[40] Thomson, A.M., West, D.C., Hahn, J., and Deuchars, J. 1996. Single axon IPSPs elicited in pyramidal cells by three classes of interneurones in slice of rat neocortex. *J. Physiol.* **496**, 81-102.

[41] Troyer, T.W. and Miller, K.D. 1997. Physiological gain leads to high ISI variability in a simple model of a cortical regular firing cell. *Neural Comput.* **9**, 733-745.

[42] Tsodyks, M., Mitkov, I., and Sompolinsky, H. 1993. Pattern of synchrony in inhomogeneous networks of oscillators with pulse interaction. *Phys. Rev. Lett.* **71**, 1282-1285.

[43] Tsodyks, M. and Sejnowski, T. 1995. Rapid state switching in balanced cortical network models. *Network* **6**, 111-124.

[44] Vaadia, E., Haalman, I., Abeles, M., Prut, Y., Slovin, H., and Aertsen, A. 1995. Dynamics of neural interaction in monkey cortex in relation to behavioral events. *Nature* **373**, 515-518

[45] van Vreeswijk, C. 1996. Partial synchrony in populations of pulse-coupled oscillators. *Phys. Rev. E* **54**, 5522-5537.

[46] van Vreeswijk, C. and Sompolinsky, H. 1996. Chaos in neuronal networks with balanced excitatory and inhibitory activity. *Science* **274**, 1724 - 1726.

[47] van Vreeswijk, C. and Sompolinsky, H. unpublished.

[48] Wilson, H.R. and Cowan, J.D. 1972. Excitatory and inhibitory interactions of localized populations of model neurons. *Biophys. J.* **12**, 1-24.